by SDS–PAGE (Laemmli, 1970) were pooled, concentrated to approximately 40 mg ml^{-1} using a centrifugal ultrafiltration tube (Amicon Ultra-15, 30 kDa cutoff; Millipore) and stored at 253 K in the presence of 50%(*v*/*v*) glycerol until the next purification step. About 5 mg of the affinity-purified protein was further purified by gel-filtration chromatography using a Superdex 200 (1 × 30 cm) column (GE Healthcare Biosciences) equilibrated with 100 m*M* phosphate buffer pH 6.8 containing 0.3 *M* NaCl and 1%(*v*/*v*) glycerol. Elution was carried out at a flow rate of 0.5 ml min^{-1} on a high-performance liquid-chromatography (HPLC) instrument. Each fraction (0.5 ml) was analyzed by SDS–PAGE and fractions containing highly pure rTbgGK were pooled. After buffer exchange to 10 m*M* MOPS buffer pH 6.8, 10 m*M* $MgSO_4$ and 1%(*v*/*v*) glycerol, the purified rTbgGK was concentrated to about 10 mg ml^{-1} for crystallization experiments. The addition of $MgSO_4$ and glycerol was crucial for preservation of the rTbgGK activity. The concentration of rTbgGK was estimated using the calculated molar extinction coefficient at 280 nm (ε_{280} = 81 080), giving an A_{280} of 1.0 for the pure rTbgGK solution at 0.74 mg ml^{-1}.

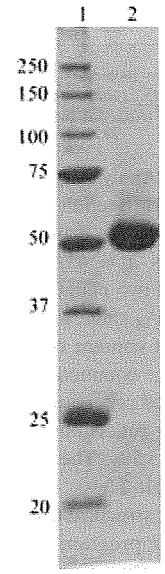

Figure 1
12.5% SDS–PAGE gel stained with Coomassie Brilliant Blue R-250 showing the apparent homogeneity of the purified rTbgGK. Lane 1, molecular-weight markers (kDa); lane 2, rTbgGK purified by Ni–NTA affinity chromatography and Superdex 200 gel filtration.

2.4. Crystallization and X-ray diffraction data collection

Crystallization conditions were initially screened at 277 and 293 K using the sitting-drop vapour-diffusion method in a 96-well Corning CrystalEX microplate with conical flat bottom (Hampton Research). A 0.5 µl droplet containing about 10 mg ml^{-1} rTbgGK dissolved in 10 m*M* MOPS buffer pH 6.8, 10 m*M* $MgSO_4$ and 1%(*v*/*v*) glycerol was mixed with an equal volume of reservoir solution and the droplet was allowed to equilibrate against 100 µl reservoir solution. In the initial screening experiment, commercially available screening kits from Hampton Research (Crystal Screen, Crystal Screen II, Grid Screen Ammonium Sulfate, Grid Screen PEG 6000, Grid Screen MPD and Quick Screen) and from Emerald BioStructures (Wizard Screen I and II) were used as the reservoir solutions. However, most of the conditions gave only heavy protein precipitates and the screening was unsuccessful. Screening was then carried out using a 5 mg ml^{-1} rTbgGK solution and twice-diluted reservoir solutions. Out of 290 conditions screened, tiny crystals and their aggregates appeared at 277 and 293 K from reservoir solutions containing 2.5–5%(*w*/*v*) PEG 6000 in the pH range 6.0–8.0. The conditions were further optimized by varying the buffer pH (5.6–8.4), the molecular weight of the PEG and its concentration [1–10%(*w*/*v*) for PEG 3350 and PEG 6000; 10–30%(*w*/*v*) for PEG 400]. Finally, single crystals suitable for X-ray diffraction experiments were obtained using a reservoir solution consisting of 30%(*w*/*v*) PEG 400 and 100 m*M* HEPES pH 7.0 within 24 h.

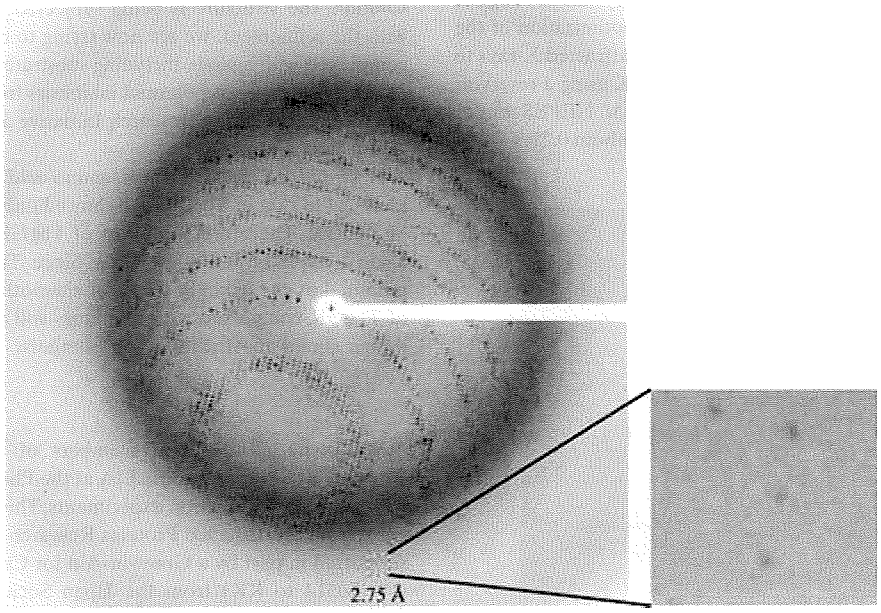

Figure 2
A typical X-ray diffraction pattern of an rTbgCK crystal. The detector edge corresponds to 2.4 Å resolution and an enlarged image of the indicated area around 2.75 Å resolution is shown. The exposure time was 1 s, with an oscillation angle of 1.0°.

X-ray diffraction experiments were performed under cryocooled conditions (100 K) on the BL41XU (λ = 1.000 Å; Rayonix MX225HE CCD detector) and BL44XU (λ = 0.900 Å; Bruker DIP-6040 detector system) beamlines at SPring-8 (Harima, Japan) and the BL17A (λ = 1.000 Å; ADSC Quantum 270 detector) beamline at the Photon Factory (Tsukuba, Japan). A crystal mounted in a nylon loop was transferred to and soaked briefly in reservoir solution containing 40%(*w*/*v*) PEG 400 and then flash-frozen at 100 K in a stream of nitrogen gas. A total of 180 images were recorded with an oscillation angle of 1.0°, an exposure time of 1 s per image and a crystal-to-detector distance of 200 mm. The diffraction data were processed and scaled with the *HKL*-2000 software package (Otwinowski & Minor, 1997).

3. Results and discussion

Gene-sequence analyses for the cDNAs of *T. b. gambiense* and *T. b. rhodesiense gk*s revealed a total of seven point differences when compared with the *gk* sequence from *T. b. brucei* (TREU927; accession No. XM_822408); only one of these differences (T212 in *T. b. brucei* to C in *T. b. gambiense* and *T. b. rhodesiense*) resulted in a change of a single amino acid (Phe71 in TbbGK to Ser71 in TbgGK and TbrGK) in the 512 amino-acid residues of TbgGK. The nucleotide-sequence data for the cDNAs of *T. b. gambiense* and *T. b. rhodesiense gk*s have been deposited in the DDBJ/EMBL/GenBank nucleotide-sequence databases with accession Nos. AB517984 and AB517985, respectively.

His_6-tagged rTbgGK with 545 amino-acid residues (60.4 kDa) was overexpressed and purified to homogeneity by a combination of Ni–NTA affinity chromatography and Superdex 200 gel-filtration chromatography (Fig. 1). About 80 mg purified enzyme with a specific activity of 31.7 µmol min^{-1} mg^{-1} was obtained from a 10 l culture. The rTbgGK protein eluted from the Superdex 200 column with a retention time corresponding to a molecular weight of about 119 kDa, indicating that the enzyme exists as a homodimer in solution.

In a screening of 290 crystallization conditions, crystals of rTbgGK were obtained using PEGs as precipitant. After optimization of the crystallization conditions, the best crystals, which diffracted X-rays to a resolution of 2.75 Å (Fig. 2), were grown at 293 K using a reservoir solution containing 30%(*w*/*v*) PEG 400 and 0.1 *M* HEPES buffer pH 7.0. The crystals attained typical dimensions of about 0.25 × 0.1 × 0.05 mm in 2 d (Fig. 3). Analysis of the symmetry and systematic absences in the recorded diffraction patterns revealed that the crystals of rTbgGK belonged to the orthorhombic space group $P2_12_12_1$, with unit-cell parameters a = 63.84, b = 121.50, c = 154.59 Å. Assuming the presence of two rTbgGK molecules (2 × 60.4 kDa) in the asymmetric unit, the V_M value was calculated to be 2.5 $Å^3$ Da^{-1}, with an estimated solvent content of 50% (Matthews, 1968); these values are within the range commonly observed for protein crystals. A total of 135 987 observed reflections recorded on 180 images were merged to 31 848 unique reflections in the 50.0–2.75 Å resolution range with an R_{merge} of 5.5%. The data-collection and processing statistics are shown in Table 1.

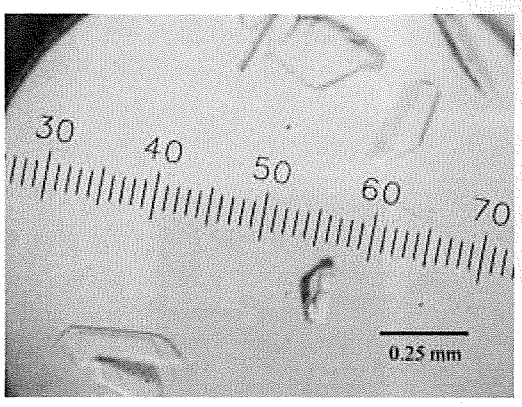

Figure 3
Crystals of rTbgGK obtained by the sitting-drop vapour-diffusion method using PEG 400 as a precipitant.

Table 1
Diffraction data statistics for the crystal of rTbgGK.

Values in parentheses are for the highest resolution shell.

Space group	$P2_12_12_1$
Unit-cell parameters (Å)	a = 63.84, b = 121.50, c = 154.59
V_M† ($Å^3$ Da^{-1})	2.5
Solvent content† (%)	50
X-ray source	BL41XU, SPring8
Wavelength (Å)	1.000
Temperature (K)	100
Resolution (Å)	50–2.75 (2.85–2.75)
Total reflections	135987
Unique reflections	31848
Completeness (%)	97.1 (95.7)
$R_{merge}(I)$‡ (%)	5.5 (46.1)
$\langle I/\sigma(I)\rangle$	18.4 (3.0)

† Assuming the presence of two molecules in the asymmetric unit. ‡ $R_{merge}(I) = \sum_{hkl}\sum_i |I_i(hkl) - \langle I(hkl)\rangle| / \sum_{hkl}\sum_i I_i(hkl)$, where $I_i(hkl)$ is the intensity of the ith observation of reflection hkl and $\langle I(hkl)\rangle$ is their average.

An attempt to solve the structure using the molecular-replacement method with the *MOLREP* program (Vagin & Teplyakov, 1997) from the *CCP*4 suite (Collaborative Computational Project, Number 4, 1994) was carried out using the refined coordinates of GK from *P. falciparum* (PDB code 2w41; 40% amino-acid sequence identity to rTbgGK; Schnick *et al.*, 2009). A promising solution with a homodimeric structure was obtained (correlation coefficient and R factor of 0.406 and 51.6%, respectively). Using the molecular-replacement solution, the structure is being subjected to refinement. In parallel with the refinement, we are now trying to obtain crystals of rTbgGK complexed with ligands, including substrates and substrate analogues. *In silico* screening of potential inhibitors from a compound library of the Chemical Biology Research Initiative at the University of Tokyo is also under way.

It should be noted that the amino-acid sequence of TbgGK was identical to that of TbrGK and showed only one difference from that of TbbGK. Therefore, inhibitors of TbgGK should also be effective against other trypanosome GKs. Since TbgGK provides a greater potential as the primary target of chemotherapy, detailed structures of TbgGK complexed with inhibitors will help structure-based drug design aimed at African trypanosomiasis.

We thank all the staff members of beamlines BL41XU and BL44XU at SPring-8 and BL17A at the Photon Factory for their help with the X-ray diffraction experiments. This work was supported by a grant from the Targeted Proteins Research Program (TPRP) and was supported in part by a Grant-in-Aid for Creative Scientific Research (18GS0314 to KK) from the Japan Society for the Promotion of Science and a Grant-in-Aid for Scientific Research on Priority Areas (18073004 to KK) from the Ministry of Education, Culture, Sports, Science and Technology, Japan. EOB is supported by a Japanese

Government Scholarship from the Ministry of Education, Science, Culture, Sports, Science and Technology.

References

Brun, R., Schumacher, R., Schmid, C., Kunz, C. & Burri, C. (2001). *Trop. Med. Int. Health*, **6**, 906–914.

Chaudhuri, M., Ott, R. D. & Hill, G. C. (2006). *Trends Parasitol.* **22**, 484–491.

Colasante, C., Ellis, M., Ruppert, T. & Voncken, F. (2006). *Proteomics*, **6**, 3275–3293.

Collaborative Computational Project, Number 4 (1994). *Acta Cryst.* D**50**, 760–763.

Fairlamb, A. H., Opperdoes, F. R. & Borst, P. (1977). *Nature (London)*, **265**, 270–271.

Guerra, D. G., Decottignies, A., Bakker, B. M. & Michels, P. A. (2006). *Mol. Biochem. Parasitol.* **149**, 155–169.

Haanstra, J. R., van Tuijl, A., Kessler, P., Reijnders, W., Michels, P. A., Westerhoff, H. V., Parsons, M. & Bakker, B. M. (2008). *Proc. Natl Acad. Sci. USA*, **105**, 17718–17723.

Hannaert, V., Bringaud, F., Opperdoes, F. R. & Michels, P. A. (2003). *Kinetoplastid Biol. Dis.* **2**, 1–30.

Hurley, J. H. (1996). *Annu. Rev. Biophys. Biomol. Struct.* **25**, 137–162.

Kido, Y., Shiba, T., Inaoka, D. K., Sakamoto, K., Nara, T., Aoki, T., Honma, T., Tanaka, A., Inoue, M., Matsuoka, S., Moore, A., Harada, S. & Kita, K. (2010). *Acta Cryst.* F**66**, 275–278.

Kralova, I., Rigden, D. J., Opperdoes, F. R. & Michels, P. A. (2000). *Eur. J. Biochem.* **267**, 2323–2333.

Laemmli, U. K. (1970). *Nature (London)*, **227**, 680–685.

Matthews, B. W. (1968). *J. Mol. Biol.* **33**, 491–497.

Michels, P. A., Hannaert, V. & Bringaud, F. (2000). *Parasitol. Today*, **16**, 482–489.

Minagawa, N., Yabu, Y., Kita, K., Nagai, K., Ohta, N., Meguro, K., Sakajo, S. & Yoshimoto, A. (1997). *Mol. Biochem. Parasitol.* **84**, 271–280.

Njiokou, F., Laveissière, C., Simo, G., Nkinin, S., Grébaut, P., Cuny, G. & Herder, S. (2006). *Infect. Genet. Evol.* **6**, 147–153.

Njogu, R. M., Whittaker, C. J. & Hill, G. C. (1980). *Mol. Biochem. Parasitol.* **1**, 13–29.

Otwinowski, Z. & Minor, W. (1997). *Methods Enzymol.* **276**, 307–326.

Schnick, C., Polley, S. D., Fivelman, Q. L., Ranford-Cartwright, L. C., Wilkinson, S. R., Brannigan, J. A., Wilkinson, A. J. & Baker, D. A. (2009). *Mol. Microbiol.* **71**, 533–545.

Singha, U. K., Peprah, E., Williams, S., Walker, R., Saha, L. & Chaudhuri, M. (2008). *Mol. Biochem. Parasitol.* **159**, 30–43.

Stevens, J. R. & Brisse, S. (2004). *The Trypanosomiases*, edited by I. Maudlin, P. Holmes & M. Miles, pp. 1–23. Wallingford: CAB International.

Van Der Meer, C. & Verslujis-Broers, J. A. (1979). *Exp. Parasitol.* **48**, 126–134.

Vagin, A. & Teplyakov, A. (1997). *J. Appl. Cryst.* **30**, 1022–1025.

World Health Organization (2006). *African trypanosomiasis*. http://www.who.int/mediacentre/factsheets/fs259/en/.

Yabu, Y., Suzuki, T., Nihei, C., Minagawa, N., Hosokawa, T., Nagai, K., Kita, K. & Ohta, N. (2006). *Parasitol. Int.* **55**, 39–43.

Biochimica et Biophysica Acta 1797 (2010) 443–450

Contents lists available at ScienceDirect

Biochimica et Biophysica Acta

journal homepage: www.elsevier.com/locate/bbabio

Purification and kinetic characterization of recombinant alternative oxidase from *Trypanosoma brucei brucei*

Yasutoshi Kido [a], Kimitoshi Sakamoto [a], Kosuke Nakamura [a], Michiyo Harada [a], Takashi Suzuki [b], Yoshisada Yabu [b], Hiroyuki Saimoto [c], Fumiyuki Yamakura [d], Daijiro Ohmori [d], Anthony Moore [e], Shigeharu Harada [f], Kiyoshi Kita [a,*]

[a] *Department of Biomedical Chemistry, Graduate School of Medicine, The University of Tokyo, Tokyo 113-0033, Japan*
[b] *Department of Molecular Parasitology, Graduate School of Medical Sciences, Nagoya City University, Nagoya 467-8601, Japan*
[c] *Department of Materials Science, Faculty of Engineering, Tottori University, Tottori, Japan*
[d] *Department of Chemistry, School of Medicine, Juntendo University, Tokyo, Japan*
[e] *Biochemistry and Biomedical Sciences, School of Life Sciences, University of Sussex, Falmer, Brighton, UK*
[f] *Department of Applied Biology, Graduate School of Science and Technology, Kyoto Institute of Technology, Kyoto 606-8585, Japan*

ARTICLE INFO

Article history:
Received 24 September 2009
Received in revised form 23 December 2009
Accepted 25 December 2009
Available online 4 January 2010

Keywords:
Alternative oxidase
Membrane-bound diiron protein
Trypanosoma brucei
Ascofuranone
Chemotherapy

ABSTRACT

The trypanosome alternative oxidase (TAO) functions in the African trypanosomes as a cytochrome-independent terminal oxidase, which is essential for their survival in the mammalian host and as it does not exist in the mammalian host is considered to be a promising drug target for the treatment of trypanosomiasis. In the present study, recombinant TAO (rTAO) overexpressed in a haem-deficient *Escherichia coli* strain has been solubilized from *E. coli* membranes and purified to homogeneity in a stable and highly active form. Analysis of bound iron detected by inductively coupled plasma-mass spectrometer (ICP-MS) reveals a stoichiometry of two bound iron atoms per monomer of rTAO. Confirmation that the rTAO was indeed a diiron protein was obtained by EPR analysis which revealed a signal, in the reduced forms of rTAO, with a *g*-value of 15. The kinetics of ubiquiol-1 oxidation by purified rTAO showed typical Michaelis–Menten kinetics (K_m of 338 μM and V_{max} of 601 μmol/min/mg), whereas ubiquinol-2 oxidation showed unusual substrate inhibition. The specific inhibitor, ascofuranone, inhibited the enzyme in a mixed-type inhibition manner with respect to ubiquinol-1.

1. Introduction

Trypanosoma brucei is a parasite that causes African sleeping sickness in humans and Nagana in livestock and is transmitted by the tsetse fly. There is an urgent need for further development of chemotherapy against African trypanosomiasis since current chemotherapeutic drugs are not entirely satisfactory [1].

Trypanosomal parasites are equipped with a unique energy metabolism, they live as the bloodstream form in the mammalian host and as the procyclic form in the vector. The procyclic form of *T. brucei* fulfills its ATP requirement from a cyanide-sensitive and cytochrome-dependent respiratory chain comparable to that observed in the host mitochondria, whereas in the bloodstream form, trypanosomes use the glycolytic pathway, which is localized in a unique organelle the glycosome, as their major source of ATP [2–5]. Once the parasites invade the mammalian host in the bloodstream form, both its cytochrome-dependent respiratory chain and ATP synthesis by oxidative phosphorylation disappear [2,5]. Instead a cyanide-resistant and cytochrome-independent trypanosomal alternative oxidase (TAO) functions as the sole terminal oxidase to re-oxidize NADH accumulated during glycolysis [5].

TAO is generally considered to be a good target for the anti-trypanosomal drugs because this oxidase is essential for their survival, since it reoxidises cytosolic NADH, and mammalian hosts do not possess this protein [5,6]. Indeed, we found that ascofuranone, isolated from the pathogenic fungus *Ascochyta visiae*, specifically inhibits the quinol oxidase activity of TAO and rapidly kills the parasites [7]. In addition, we have confirmed the chemotherapeutic efficacy of ascofuranone *in vivo* [8,9].

The alternative oxidase (AOX) is a non-protonmotive ubiquinol oxido-reductase catalyzing the 4-electron reduction of dioxygen to water [5,10–12]. Genes encoding AOX have been found in higher

Abbreviations: AOX, alternative oxidase; DM, *n*-dodecyl-β-D-maltopyranoside; EPR, electron paramagnetic resonance; ICP-MS, inductively coupled plasma-mass spectrometer; IPTG, isopropyl, β-D-1-thiogalactoside; k_{cat}, molecular activity; C10E8, octaethylene glycol-monododecylether; OG, *n*-octyl-β-D-glucopyranoside; rTAO, recombinant trypanosome alternative oxidase; SHAM, salycylhydroxamic acid; TAO, trypanosome alternative oxidase; Ubiquinol, reduced form ubiquinone

* Corresponding author. Department of Biomedical Chemistry, Graduate School of Medicine, The University of Tokyo, Hongo, Bunkyo-ku, Tokyo 113-0033, Japan. Tel.: +81 3 5841 3526; fax: +81 3 5841 3444.
E-mail address: kitak@m.u-tokyo.ac.jp (K. Kita).

0005-2728/$ – see front matter © 2009 Elsevier B.V. All rights reserved.
doi:10.1016/j.bbabio.2009.12.021

plants, algae, yeast, slime molds, free-living amoebae, eubacteria and nematodes [13–16]. Moreover, recent bioinformatic searches have broadened the taxonomic distribution of AOX to some members of the animal kingdom [17]. The primary role of AOX in non-thermogenic plants is to regulate cellular redox balance and to protect against reactive oxygen species particularly when the cytochrome pathway is inhibited [18–20]. In addition to this role, many other physiological roles have been described for AOXs in other organisms and these have been discussed in detail elsewhere [13,21]. The ubiquitous occurrence of AOX may suggest that the metabolic flexibility that the alternative pathway confers upon an organism allows it to respond to a wide range of developmental and environmental conditions [22].

Despite universal conservation of the gene and diversified physiology, the molecular features of AOX have not yet been well characterized. Although no high-resolution AOX structure has been determined to date, current structural models predict that it is an integral interfacial membrane protein that interacts with a single leaflet of the lipid bilayer, and contains a non-haem diiron carboxylate active site [23,24]. This model is supported by extensive site-directed mutagenesis studies [18,25–29] and furthermore both EPR and FTIR spectroscopies have confirmed the presence of a binuclear iron center in both the plant and trypanosomal enzymes [30–32].

Further detailed structural and biochemical analyses of AOXs, however, requires further development of purification protocols to produce sufficiently purified and highly active protein to enable crystallization trials and kinetic analyses to proceed. In this paper, we report on the further refinement of our previous protocol through over-expressing rTAO in an *E. coli ΔhemA* mutant (FN102) strain, which lacks quinol oxidase activity of cytochrome *bo* and *bd* complexes [33–35]. Purified rTAO protein is highly active and exhibits an exceptional stability upon storage. The analysis of the prosthetic groups by inductively coupled plasma-mass spectrometer (ICP-MS) and electron paramagnetic resonance (EPR) reveals the presence of two ferric ions stoichiometrically bound per rTAO monomer. To our knowledge this is the first direct confirmation of two ferric irons per AOX. Furthermore we show that purified rTAO is potently inhibited by ascofuranone with mixed function kinetics.

2. Materials and methods

2.1. Preparation of membrane sample

The strain FN102/pTbAO carrying cDNA for *T. b. brucei* TAO [36] was pre-cultured at 37 °C in 100 ml of LB medium containing 10 mg ampicillin, 5 mg kanamycin, and 5 mg 5-aminolevulinic acid for 4–6 h. The pre-cultured cells were aerobically grown at 30 °C in 10 l of S-medium containing 100 g tryptone peptone, 50 g yeast extract, 50 g casamino acid, 104 g K_2HPO_4, 30 g KH_2PO_4, 7.5 g trisodium-citrate·$2H_2O$, 25 g $(NH_4)_2SO_4$, 0.5 g $MgSO_4 \cdot 7H_2O$, 0.25 g $FeSO_4 \cdot 7H_2O$, 0.25 g $FeCl_3$, 0.2%(w/v) glucose, and 1 g carbenicillin. The culture was initiated at O.D.$_{600}$ = 0.01 and expression of rTAO was induced by the addition of isopropyl β-D-1-thiogalactoside (IPTG) (25 μM) at O.D.$_{600}$ = 0.1. Cells were harvested 8–10 h following induction and were resuspended in 50 mM Tris–HCl (pH 7.5) containing 20%(w/w) sucrose, 0.1 mM phenylmethane sulfonyl fluoride (PMSF) and protease inhibitor cocktail (Sigma) and broken by a French Pressure Cell (Ohtake, Tokyo). Unbroken cells were removed by centrifugation at 8000 *g* for 10 min (Hitachi 21G). Inner membranes of FN102/pTbAO were fractionated in high density sucrose after ultracentrifugation at 200,000 *g* for 1 h at 4 °C (Hitachi 85H) (35 ml of supernatant was overlaid over 35 ml of 50 mM Tris–HCl pH 7.5 containing 40%(w/w) sucrose per ultracentrifuge tube). Buoyant inner rich membranes upon 40%(w/w) sucrose layer were fractionated and the inner membrane pellet was separated by further ultracentrifugation at 200,000 *g* for 1 h (HITACHI 85H). The membrane pellet was resuspended in 50 mM Tris–HCl (pH 7.5) containing 20%(w/w) sucrose.

2.2. Solubilization

Membranes were treated with solubilization buffer (6 mg/ml protein in 50 mM Tris–HCl, 1.4%(w/v) *n*-octyl-β-D-glucopyranoside (OG), 200 mM $MgSO_4$, 20%(v/v) glycerol, pH 7.3) at 4 °C and immediately ultracentrifuged at 200,000 *g* for 1 h at 4 °C. The quinol oxidase activities of the samples before centrifugation, as well as that of supernatant and pellet were determined.

2.3. Purification of rTAO

Hybrid batch/column procedure described in the manufacturer's instruction was used as stated below. Ten milliliter of the resin (BD Bioscience, TALON Metal Affinity Resin) was equilibrated in a batch format by 100 ml of equilibration buffer (20 mM Tris–HCl, 1.4%(w/v) OG, 100 mM $MgSO_4$, 20%(v/v) glycerol, pH 7.3). Twenty milliliter of OG extract was mixed with the resin for 20 min at 4 °C. The resin was washed twice with 100 ml of wash buffer (20 mM Tris–HCl, 20 mM imidazole, 0.042%(w/v) *n*-dodecyl-β-D-maltopyranoside (DM), 50 mM $MgSO_4$, 20%(v/v) glycerol pH 7.3) and the resin bound rTAO was transferred to a column for additional washing with 20 ml of second wash buffer (20 mM Tris–HCl, 165 mM imidazole, 0.042%(w/v) DM, 50 mM $MgSO_4$, 20%(v/v) glycerol pH 7.3; flow rate 1 ml/min) and protein elution. Finally, rTAO was eluted with elution buffer (20 mM Tris–HCl, 200 mM imidazole, 0.042%(w/v) DM, 50 mM $MgSO_4$, 60 mM NaCl, 20%(v/v) glycerol pH 7.3; flow rate 1 ml/min). Fractions (4 ml each) were collected.

2.4. Quantitative analysis of metals and EPR spectroscopy

Three independent preparations of rTAO were analyzed (details in Section 3). Each sample solution containing 0.1 g of rTAO was added to 1 ml of nitric acid and 7 ml of water. Organic compounds were hydrolyzed by microwave-assisted protein digestion system (Ethos Pro, Milestone General). Fe, Mn, Cu, Zn and Co in each sample were quantified by inductively coupled plasma-mass spectrometer (ICP-MS, ELAN DRC PerkinElmer Japan). Analysis was performed by the Sumika Chemical Analysis Center (Osaka, Japan). Protein concentration was determined by the Lowry method.

EPR spectra were recorded on a JEOL X-band JES-FA300 spectrometer equipped with an ES-CT470 Heli-Tran cryostat system and a Scientific Instruments digital temperature indicator/controller model 9700a. For EPR analysis of rTAO, 13 mg/ml purified rTAO was frozen in EPR tubes in liquid nitrogen. The purified rTAO was reduced by 2 mM dithionite and 1 mM phenazine methosulfate prior to freezing.

2.5. Ubiquinol oxidase assay

Ubiquinol oxidase activity was measured by recording the absorbance change of ubiquinol-1 at 278 nm (Shimadzu spectrophotometer UV-3000). Reactions were started by the addition of ubiquinol-1 (final concentration 150 μM, $\varepsilon_{278} = 15{,}000\ M^{-1}\ cm^{-1}$) after 2 min preincubation at 25 °C in the presence of rTAO and 50 mM Tris–HCl (pH 7.4). For the enzyme kinetics of purified rTAO, the reaction was initiated by the addition of ubiquinol-1 after 2 min preincubation at 25 °C in the presence of rTAO and 50 mM Tris–HCl (pH 7.4) containing 0.05%(w/v) octaethylene glycol-monododecylether detergent (C10E8).

2.6. Chemicals

All chemicals were biochemistry grade. Ubiquinone-1 and protease inhibitor cocktail were purchased from Sigma-Aldrich. The other detergents were purchased from Dojin Chemicals (Tokyo, Japan).

3. Results

3.1. Purification of fully active TAO

Although we previously established a protocol for the overproduction of rTAO in *E. coli* FN102 (*ΔhemA*) lacking cytochrome *bo* and *bd* complexes of the bacteria, the yield of the active enzyme was too low to analyze its prosthetic group [36]. Such a preparation also hampered the determination of kinetic parameters of rTAO such as its molecular activity. Therefore, conditions for the expression of rTAO and purification protocols were optimized to obtain large quantities of active and stable rTAO to enable such determinations. Three factors were critical to obtain large amounts of active rTAO, namely, growth time of the culture prior to addition of IPTG, absolute concentration of IPTG, and the use of purified inner membranes as the starting material.

After extensive screening of detergents and additives to establish the procedure for efficient extraction of active rTAO from the inner membranes, we found that *n*-octyl-β-D-glucopyranoside (OG) specifically solubilized rTAO as shown in Table 1 (specific activity increased from 23.3 to 63.2 μmol/min/mg after solubilization). Approximately 60% of the membrane quinol oxidase activity was recovered with 1.4%(w/v) OG in the extract (Sup. Fig. 1). Thus, recovery of the activity was significantly higher than that of previously reported digitonin extraction (17%) [36]. Following solubilization, it was possible to maintain enzymatic activity for at least 1 month at 20 °C.

Since rTAO was fused with N-terminal histidine tag, solubilized rTAO was purified by cobalt affinity chromatography. Although the enzyme solubilized by OG was bound to the cobalt affinity resin in the presence of OG, it was not possible to elute bound rTAO from the resin with buffer containing OG. Interestingly, however, we found that 100% of the rTAO activity could be recovered from the column when OG in the washing and elution buffers was exchanged with *n*-dodecyl-β-D-maltopyranoside (DM). In the final step, purified rTAO was obtained by a two-step elution with 165 mM and 200 mM imidazole, which resulted in a very efficient purification of active rTAO in the presence of DM. A typical elution profile of quinol oxidase activity with increasing imidazole concentration is shown in Sup. Fig. 1B. Purified rTAO, with a molecular mass of 34 kDa, was estimated to be 95% pure by SDS-PAGE (Fig. 1A, lane 5). In addition to the 34 kDa band, it is apparent that other bands are also present including two with a smaller size than rTAO and one band with an approximate molecular mass of 74 kDa. Since all of these bands were recognized in Western blot using a monoclonal antibody against TAO (Fig. 1B), the smaller protein bands possibly represent proteolytic breakdown products whilst the 74 kDa band most likely represents the dimeric form of rTAO. The specific activity of purified rTAO was more than 200 μmol/min/mg protein when 150 μM of ubiquinol-1 was used as a substrate, which had a five-fold higher activity than that of the previously purified rTAO (approximately 40 μmol/min/mg) [36]. Quinol oxidase activity of purified rTAO was insensitive to 5 mM KCN but was completely inhibited by 10 nM ascofuranone. A greater than 35-fold increase in purification was achieved using the techniques described above, and 13.2% of the total activity was recovered from the lysate of FN102/pTAO cells as summarized in Table 1. Such procedures resulted in approximately 10 mg of highly purified rTAO from a 10 l culture.

Table 1
Purification of rTAO.

Fractions	Total activity (μmol/min)	Protein (mg)	Specific activity (μmol/min/mg)	Recovery (%)
E. coli lysate	14100	2410	5.85	100
Inner membrane	3500	150	23.3	24.8
OG extract	2400	37.9	63.2	17.0
Co-column	1860	8.95	207	13.2

The activities listed here were measured using 150 μM of ubiquinol-1. Fractions (eluate numbers 6–13 in Supplemental Fig. 1B) were collected as purified rTAO after co-column.

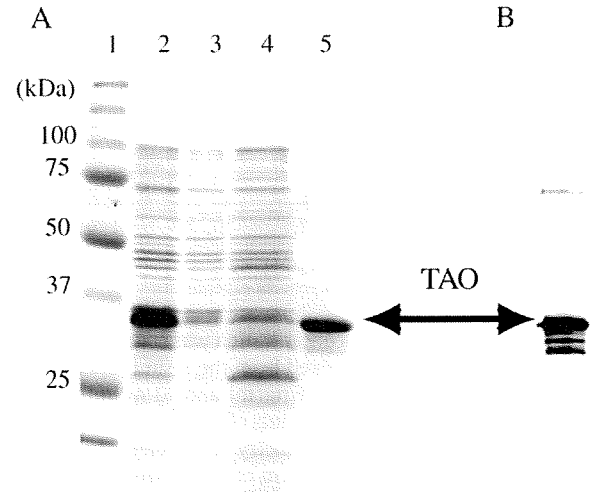

Fig. 1. SDS-PAGE and Western blotting of rTAO in purification steps. A: CBB-staining 12.5% SDS-PAGE of each fraction from the cobalt column chromatography. Lane 1, marker; lanes 2 and 3, each 5 ml of OG extract and flow through fraction; lane 4, 500 ml of wash fraction; and lane 5, 60 ml of eluted fraction collected from fractions 6–12. Loading samples on lanes 2 to 5 were precipitated with acetone. B: Western blot of purified rTAO. The same sample to lane 5 in panel B was electrophoresed on 12.5% polyacrylamide gel. Monoclonal antibodies were used against highly purified rTAO obtained by a nickel column in the presence of guanidine. Epitope recognized by this antibody is the C-terminal domain of the enzyme. The arrow indicates rTAO with an apparent molecular mass of 34 kDa.

3.2. Iron content in purified TAO

Since a highly active and stable purified rTAO could be obtained by the protocol described above, the metal content of purified rTAO was measured by ICP-MS. On the basis that TAO has a diiron center as previously proposed [23,24], then two equivalents of iron should be detected per monomer of rTAO. To this end we analyzed the iron content of purified native rTAO, inactive rTAO, denatured rTAO, and iron within the buffer eluted from the cobalt-column. Purified native rTAOs derived from three independent *E. coli* cultures were precipitated by PEG 3350 and resuspended in the elution buffer at three different concentrations as shown in Sup. Table 1. To prepare inactive rTAO, precipitated rTAO was resuspended in 50 mM Tris–HCl pH 7.4, which resulted in complete loss of enzyme activity. Denatured rTAO was prepared by resuspending the precipitant in elution buffer containing 6 M guanidine–HCl and 0.3 M EDTA. Metal contents in these preparations were 9000 ng/ml, 2900 ng/ml and 1800 ng/ml of Fe respectively for the native rTAO (3.71, 1.19 and 0.80 mg/ml), 230 ng/ml, 100 ng/ml and 28 ng/ml of Fe for inactive rTAO, denatured rTAO and the elution buffer, respectively (Sup. Table 1). From these results, the stoichiometry of bound iron per rTAO monomer can be deduced as indicated below, based on the following parameters namely, a molecular mass of rTAO of 39,391 Da (including the 6× histidine tag), purity of 95% based on SDS-PAGE gels, and the atomic weight of Fe being 55.85. Thus the ratio of iron atoms per rTAO is 1.76 for native rTAO and 0.2 and 0.08 in inactive rTAO and denatured rTAO, respectively (Table 2). This data indicates that one monomer of TAO possesses two atoms of iron which are released during inactivation or denaturation of the enzyme. To our knowledge, this is the first direct measurement of iron in purified AOX and the stoichiometry is consistent with the active site of AOX being a diiron carboxylate-center.

Other metals including Mn, Cu and Zn were also analyzed (Sup. Table 1). In all cases, these metals were below their detection limit (10 ng/ml sample solution) or background level. Although cobalt was

Table 2
Ratio of metals to purified rTAO.

	Fe/rTAO	Zn/rTAO	Mn/rTAO	Cu/rTAO
	Mean ± S.D.			
Native rTAO	1.76 ± 0.077	0.03 ± 0.013	N.D.[a]	N.D.
Inactive rTAO	0.22[b]	N.D.	N.D.	N.D.
Denatured rTAO	0.08[b]	N.D.	N.D.	N.D.

Stoichiometric ratio of metals to one molecular TAO was calculated using data in Supplemental Table 1.
[a] N.D. represents Not Detected (below 0.01).
[b] The value is an average of two independent experiments.

detected in purified rTAO, its concentration was comparable to that of cobalt in the elution buffer derived from the resin (data not shown). Similarly although 130 ng/ml, 66 ng/ml and 61 ng/ml of Zn were detected in native rTAO, these amounts of Zn were not commensurate with that of the enzyme stoichiometry. The detected Zn might be derived from the Zn-substituted form of rTAO, which was suggested to be possible from structural analysis [37]. In addition, at least 90% of the purified rTAO retained its prosthetic group in its active form.

In addition to measuring the stoichiometry of iron in purified rTAO, EPR analysis of purified rTAO was also performed in order to confirm that purified rTAO was indeed a diiron carboxylate protein and whether the detected iron originated from a diiron binding center. As shown in Fig. 2, a low field EPR signal at approximately $g = 15$ in the perpendicular EPR mode was observed with the reduced form of rTAO when the enzyme was reduced by 2 mM of dithionite and 1 mM of phenazine methosulfate (PMS), although the intensity of the signal was low. Importantly the signal disappeared in the oxidized form of rTAO. This low field EPR signal is characteristic for diiron proteins and is ascribed to an exchange-coupled high spin ferrous iron [38]. Although this signal is not normally observed in the perpendicular mode, it can be detected under certain conditions as outlined in this report [39]. The effective g-value of 15 observed in the perpendicular mode is slightly lower than the value of 16 previously observed by us [31] but this is probably due to the fact that parallel-mode EPR spectroscopy is a much more sensitive probe than the perpendicular mode. Nevertheless the finding of a low field signal when the purified enzyme is reduced is further confirmation that the purified rTAO we report here is indeed a diiron carboxylate protein. It should be noted however that we were unable to observe the $g = 15$ signal when the enzyme was reduced by more physiological reductants such as ubiquinol-1 the reasons for which are, at present, unclear.

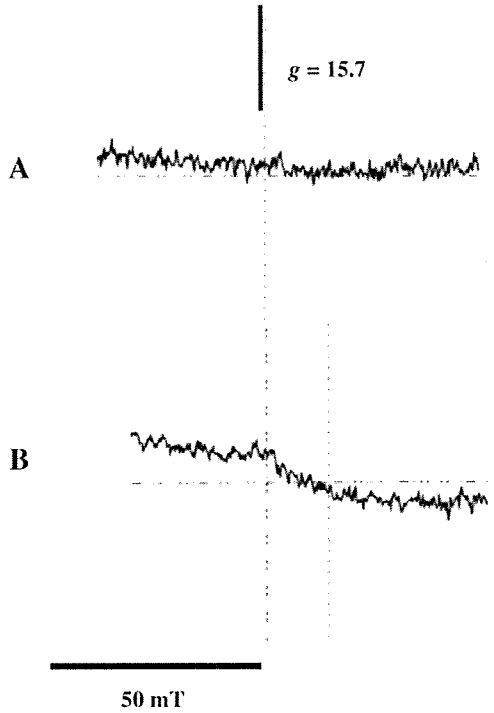

Fig. 2. EPR spectra of rTAO. A: Oxidized form of rTAO (360 μM). B: Reduced form of rTAO (360 μM), which was treated by 2 mM of dithionite and 1 mM phenazine methosulfate for 30 min on ice. Instrument parameters: microwave frequency, 9.02 GHz; microwave power, 1 mW; modulation frequency, 100 kHz; modulation amplitude, 0.6 mT; and temperature of 5 K.

3.3. Kinetic properties of purified TAO

Kinetic analysis of purified rTAO (or AOX) using ubiquinone analogs has previously proved difficult because: 1) the enzyme, following solubilization, was extremely unstable, 2) the natural substrate of trypanosome AOX is ubiquinol-9 [4], which is too hydrophobic to use as the substrate in the assay and 3) the enzymatic activity was not saturated at the maximum concentration of ubiquinol-1 (approximately 300 μM). Since we have purified rTAO in a fully active form and confirmed the stoichiometric presence of the diiron center, the purified rTAO was well-suited to a kinetic analysis.

As noted in our earlier study [36] and in AOXs from other organisms [40] non Michaelis–Menten kinetics is observed when ubiquinol-1 is used as a substrate. Hoefnagel et al. [40], however, observed that the addition of a specific detergent (0.025% EDT-20) during the assay increased the activity by 3- to 4-fold close to saturation. Although the addition of 0.025%(w/v) of EDT-20 equally enhanced the activity of purified rTAO by approximately 2-fold, it did have a deleterious effect upon the long term stability of the enzyme (Sup. Fig. 2).

In an attempt to overcome this problem, various detergents were therefore screened to determine if they could enhance activity without affecting enzyme stability. When the effect of the detergents on enzyme activity was evaluated by monitoring the activity of rTAO in the presence of detergent (Sup. Fig. 3), most activity was retained in the presence of 0.05%(w/v) of C10E8 (Sup. Fig. 4A). Light scattering at 400 nm confirmed that at least 600 μM of ubiquinol-1 was soluble in the assay system (Sup. Fig. 4B). The kinetics of ubiquinol-1 oxidation by purified rTAO in the presence of 0.05%(w/v) of C10E8 showed typical Michaelis–Menten kinetics (Fig. 3, K_m of 338 ± 23.2 μM and V_{max} of 601 ± 27.0 μmol/min/mg). In contrast, activity was linearly dependent upon substrate concentration in the absence of detergent indicating unsaturation in agreement with previous studies [36,40] (Fig. 4). Enzymatic analysis was performed with a wide range of

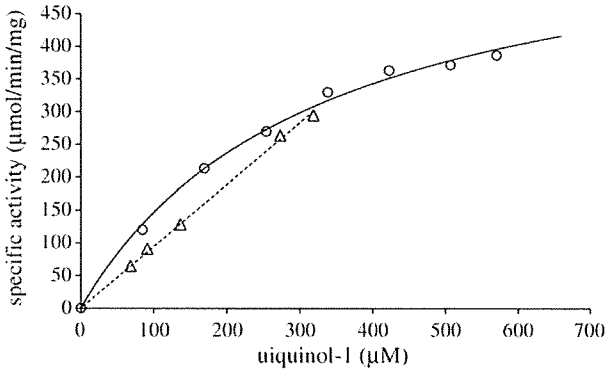

Fig. 3. Kinetics of ubiquinol-1 oxidation by purified rTAO. S–V plot of ubiquinol oxidase activity is shown using 75 ng of purified rTAO in 50 mM Tris–HCl (pH 7.4) and ubiquinol-1 (80–580 μM) with (○) and without (△) 0.05%(w/v) C10E8 at 25 °C. The solid line indicates the fitted Michaelis–Menten kinetics with the detergent (K_m of 338 ± 23.2 μM and V_{max} of 601 ± 27.0 μmol/min/mg), whereas the dashed line indicates the linear relationship between the substrate concentration and the activity without the detergent.

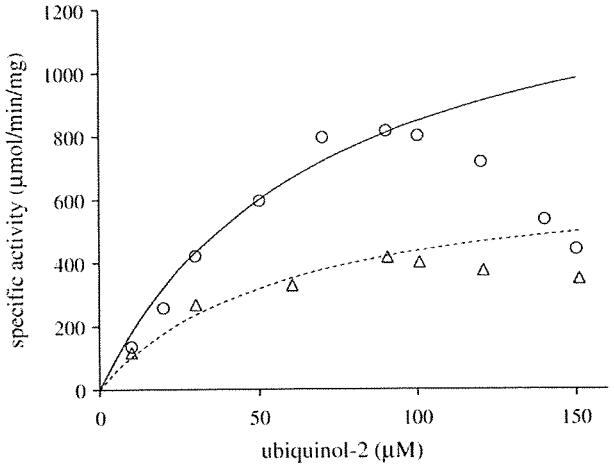

Fig. 4. Kinetics of ubiquinol-2 oxidation by purified rTAO. S–V plot of ubiquinol oxidase activity is shown using 75 ng of purified rTAO in 50 mM Tris–HCl (pH 7.4) and ubiquinol-2 (10–150 μM) with (△) 0.05%(w/v) C10E8 and with (○) 0.025%(w/v) EDT-20 at 25 °C. The solid line indicates the fitted Michaelis–Menten kinetics in the concentration range below 90 μM of ubiquinol-2 with 0.025%(w/v) EDT-20, whereas the dashed line does with 0.05%(w/v) C10E8 (K_m of 71 ± 1.2 μM and V_{max} of 1,460 ± 53.2 μmol/min/mg with 0.025%(w/v) EDT-20, whereas K_m of 57 ± 8.5 μM and V_{max} of 691 ± 28.0 μmol/min/mg with 0.05%(w/v) C10E8).

substrate concentrations (80–570 μM), which corresponded to 0.4 K_m–1.7 K_m.

To investigate whether the length of the side chain of the substrate affected the kinetic properties of rTAO, a kinetic analysis using ubiquinol-2 in the presence of EDT-20 and C10E8 (Fig. 4) was performed. Fig. 4 indicates that during the oxidation of ubiquinol-2, enzyme activity decreased above 100 μM substrate even in buffers containing either detergent. Although kinetic parameters using ubiquinol-2 could not be obtained due to substrate inhibition, S–V plots in the concentration range below 90 μM of ubiquinol-2 could be used to qualitatively analyze the effects of side chain on enzyme activity. Calculated values from such plots revealed that in the presence of 0.025%(w/v) EDT-20 the K_m (ubiquinol-2) was 71 ± 1.2 μM and V_{max} = 1460 ± 53.2 μmol/min/mg whereas with, 0.05%(w/v) C10E8 the K_m was 57 ± 8.5 μM and V_{max} = 691 ± 28.0 μmol/min/mg.

Ascofuranone is a highly specific and potent inhibitor of TAO [7] and it was therefore of importance to determine its inhibitory effect on ubiquinol-1 oxidation by purified rTAO in the presence of 0.05%(w/v) of C10E8 (Sup. Fig. 5A). From the data presented in Sup. Fig. 5A the apparent kinetic parameters of ubiquinol-1 oxidation in the presence of 0.5 nM and 2 nM of ascofuranone were estimated to be respectively $K_m^{0.5\,nM}$ = 368 ± 6.4 μM; $V_{max}^{0.5\,nM}$ = 490 ± 22.4 μmol/min/mg and $K_m^{2\,nM}$ = 492 ± 7.2 μM; and $V_{max}^{2\,nM}$ = 309 ± 60.5 μmol/min/mg. The increased K_m and decreased V_{max} values (Sup. Fig. 5B) indicate that ascofuranone inhibits purified rTAO in a mixed-type non-competitive manner with respect to ubiquinol-1.

4. Discussion

The overall goal of the present study was to obtain a highly pure and stable rTAO protein with maximum specific activity which could be used to investigate the kinetic properties of the enzyme. The quality of the purified rTAO obtained in this study has resulted in three important aspects with respect to the structure of AOX namely, the first direct evidence of stoichiometrically bound iron within the diiron center of rTAO, secondly reliable measurements of kinetic parameters and thirdly that a sample of sufficient purity and yield could be produced that has resulted in the formation of crystals [41].

4.1. Overexpression and purification of rTAO

The difficulties in isolating stable AOXs in an active form have hampered the biochemical and structural analyses of the enzyme including identification of its prosthetic groups, tertiary structural analysis and the definition of enzyme kinetic parameters. The present study reports on the overexpression and purification of active rTAO, which has enabled us to study biochemical and protein chemistry properties of this enzyme. The protocol described in this paper results in the purification of large amounts of stable rTAO with high specific activity. Two factors appeared critical to functionally express highly active rTAO. Firstly, the optimization of culture conditions, including culture duration and IPTG concentration, was crucial for the successful overexpression of rTAO with high specific activity. Secondly, activity was maximized when rTAO was purified from *E. coli* inner membranes—activity decreased substantially when it was isolated from an unpurified membrane fraction. Additionally, changing the detergent from OG to DM following solubilization, also appeared important to maximize yield and activity. Purified rTAO produced in this manner retained complete activity for more than 6 months at 4 °C and for more than 1 month at 20 °C. Furthermore, we have also been able to purify *Sauromattum guttatum* rAOX by this procedure showing the universality of the purification protocol (Elliott, C.E., Kido, Y., Kita, K. and Moore, A.L. unpublished observations).

It is anticipated that highly purified and active AOX will open a new direction with respect to the investigation of the structure and reaction mechanisms of AOXs and contribute to further progress on the study of this novel terminal oxidase. Indeed we recently took advantage of the exceptional stability and purity of the rTAO by performing the first FTIR spectroscopic investigation of any diiron protein [32]. Stepwise reduction of the fully oxidized resting state of rTAO revealed two distinct IR redox difference spectra. The first of these, "signal 1", contained clear features that could be assigned to protonation of at least one carboxylate group, further perturbations of carboxylic and histidine residues, bound ubiquinone and a negative band that might arise from a radical in the fully oxidized protein. A second IR redox difference spectrum, "signal 2", appeared more slowly (within approximately 1 h) once signal 1 had been reduced and is quite distinct from the components which comprise signal 1. The exact identity of the components which result in signal 2 await further investigations. Such a study has not previously been possible with AOX preparations because of protein instability at room temperature.

4.2. Prosthetic group analysis

Prosthetic group analysis summarized in Table 2 revealed that in highly stable and purified rTAO there are two equivalents of iron per rTAO monomer with no other metals, including Cu, Mn and Zn, being detected. EPR spectroscopy confirms that the irons are part of a diiron center since an EPR signal at $g = 15$ could be detected (Fig. 2) when rTAO is reduced by dithionite in the presence of PMS. The fact that this signal can be detected in all AOXs examined to date suggests that the signal is a characteristic signature of AOXs [30,31] and in agreement with mutational analyses [18,25–29] is further confirmation that TAO, similar to AOXs in other organisms, is a diiron carboxylate protein. Furthermore the data summarized in Table 2 revealed that when the protein was either inactivated or denatured iron was released indicating it is essential for TAO activity. Moreover, this data has established biochemically the validity of predicting the presence of a diiron center from amino acid sequence data, not only in AOX but also in other membrane-bound diiron carboxylate proteins including 5-demethoxyquinone hydroxylase (CLK-1/Coq7) (which also has the diiron binding motif EXXH). It is of interest to note that both AOX and CLK-1/Coq7 utilize ubiquinol as substrate and both are involved in respiration [42–44].

4.3. Kinetic analysis

The inclusion of C10E8 in the assay was found to be critical for the kinetic analysis of TAO and the evaluation of inhibitors. In Table 3, we have calculated fundamental kinetic parameters of TAO and compared them to those of *E. coli* cytochrome *bo* oxidase complex and *S. cerevisiae* ubiquinol–cytochrome *c* reductase [45]. These kinetic constants provide a molecular rationale on how the alternative pathway can effectively compete with other terminal oxidases, although caution must be exercised in the interpretation of this data as it is derived from experiments performed under non-physiological conditions and substrates. Nevertheless Table 3 indicates that TAO has a calculated k_{cat} of $415 \pm 19\ s^{-1}$ (on the basis that the purity of rTAO is 95%), which is slightly higher than that of the cytochrome *bo* oxidase complex ($313\ s^{-1}$), yeast ubiquinol–cytochrome *c* reductase ($153\ s^{-1}$) and previous values reported for the plant AOX ($186\ s^{-1}$), but considerably less than that calculated for cytochrome *c* oxidase ($770\ s^{-1}$) [45–48]. Taking into account that the value of the specificity constant (k_{cat}/K_m) of enzymatic reactions is known to be less than $10^9\ M^{-1}\ s^{-1}$ (from the perspective of diffusion limited access of substrates [49]), it is apparent from Table 3 that both cytochrome *bo* oxidase and TAO have quite high and comparable catalytic activities. These values suggest that the activation energy of both quinol oxidase reactions are similar and furthermore that the quinol oxidase activity of TAO is thermodynamically "alternative" to that of the cytochrome *bo* complex. In contrast however, TAO does not appear to compete effectively with the bc_1 complex in terms of specificity constant and, if the plant AOX possesses a similar specificity constant to that of TAO, it would suggest that plant alternative oxidase activity would be severely curtailed unless the conventional respiratory chain is limited either through inhibition (which appears to be the case under 'stressed conditions') or through down regulation as appears to be the case in thermogenic tissues [12,50,51].

Interestingly ubiquinol-2 oxidation by rTAO showed substrate inhibition at concentrations above 100 μM in a manner similar to that observed when the heterodimeric terminal ubiquinol oxidase of *E. coli*, cytochrome *bd* oxidized ubiquinol-2 as substrate [52]. A lower K_m value of ubiquinol-2 than that of ubiquinol-1 might be related not only to its hydrophobicity but also could be a function of the isoprenoid chain. The peculiar kinetics of ubiquinol-2 might be attributed to the following two points; 1) competition for the ubiquinol-2 oxidation site between the substrate and the product, and 2) the presence of inactive intermediates of the enzyme related to the precise catalytic mechanism.

Kinetic analysis of the mechanism of inhibition by the specific TAO inhibitor ascofuranone (Sup. Fig. 5) indicates that it is a mixed-type inhibitor with respect to ubiquinol-1. The discrepancy between the mixed inhibition observed in this report and competitive inhibition as reported in our previous study [36] might be due to the different assay conditions used in the experiments described in this paper. In the previous study, the kinetic parameters were based on apparent values because enzymatic activity was calculated without detergents and hence only low ranges of ubiquinol-1 concentrations (0.01 K_m–0.3 K_m) could be used. In contrast, the kinetic parameters reported in the current study were determined with much higher reliability since in the presence of C10E8, a much wider range of ubiquinol-1 (0.4 K_m–1.7 K_m) could be used.

Table 3
Kinetic parameters of quinol oxidases (with respect to ubiquinol-1).

	K_m (μM)	V_{max} (μmol/min/mg protein)	k_{cat} (s^{-1})	k_{cat}/K_m ($\mu M^{-1}\ s^{-1}$)
TAO[a]	338 ± 23.2	601 ± 27.0	415 ± 19	1.2
Cyt *bo* oxidase[b]	61	–	313	5.2
Ubiquinol-cyt *c* reductase[c]	13	–	220	16.9

The k_{cat} value of cytochrome *c* oxidase is $k_{cat} = 770\ (s^{-1})$ [46].
All the k_{cat} values listed here were obtained by dividing the V_{max} by the concentration of the enzymes (mol/mg protein).
[a] This study.
[b] *E. coli* cytochrome *bo* oxidase as in Sakamoto et al. [47].
[c] Ubiquinol–cytochrome *c* reductase from bovine heart as in Fato et al. [45].

4.4. Unique feature of AOX

AOX is found in various organisms and recent genome database searches have also identified AOX in different phyla of the Animalia kingdom (Mollusca, Nematoda and Chordata) [17]. It has been suggested that since AOX is absent from mammalian tissues TAO could be a chemotherapeutic target, since it functions in the bloodstream form of *T. brucei* as the only terminal oxidase and hence is essential for the survival of trypanosomes [5,6]. As an AOX protein has also been identified in *Cryptosporidium parvum* [53,54], which causes diarrheal disease cryptosporidiosis, and the recombinant *C. parvum* AOX is also sensitive to ascofuranone and as a result suggests that not only could AOX be a potential drug target in a number of parasites but furthermore ascofuranone could be used to treat a number of infections since this compound shows potent, broad-spectrum antimicrobial activity [53].

In addition to this clinical application, there is considerable interest in the unique characteristics of the enzyme since the functions and properties of TAO are clearly distinct from those of other bacterial quinol oxidases. TAO is a cytochrome-independent and cyanide-insensitive quinol oxidase, whereas cytochrome *bo* and *bd* complexes are cytochrome-dependent and cyanide-sensitive quinol oxidases [34,35]. Furthermore, TAO has various other physiological roles in *T. brucei*; the cytochrome and alternative pathways are both active and functional in the procyclic forms [55] in addition to the bloodstream form, thereby possibly providing metabolic flexibility under changing environmental conditions. TAO activity also appears to regulate the expression of one of the major surface coat proteins, GPEET, in the procyclic form [56], and in addition may regulate the observed programmed cell death-like phenomena in the bloodstream forms [57].

5. Conclusions

The primary aim of our research on TAO is to elucidate the interaction between the enzyme and its substrate or inhibitor, which hopefully could act as a structural guide for ongoing drug development. In addition to the knowledge obtained from this study, further studies on the inhibitory kinetics and structure–activity relationship of ascofuranone derivatives, along with mutational analyses of TAO [27,29] and X-ray structure analysis will undoubtedly have considerable implications with respect to our understanding of how the enzyme interacts with its substrate and inhibitors. A three-dimensional structure of TAO with and without ascofuranone should also shed light on the inhibitory mechanism of this potent drug, which according to this study occurs via a mixed-type inhibition. Such further insights about the interaction between ascofuranone and the enzyme will hopefully lead to a more rational design of more potent and safe anti-trypanosomal drugs.

Acknowledgements

This work was supported in part by Grant-in-aid for Young Scientists (B) 21790402 (to YK), Grant-in-Aid for Scientific Research (C) 21590467 (to YY), Creative Scientific Research Grant 18GS0314 (to KK), Grant-in-aid for Scientific Research on Priority Areas 18073004 (to KK) from the Japanese Society for the Promotion of Science, and Targeted Proteins Research Program (to KK) from the

Japanese Ministry of Education, Science, Culture, Sports and Technology (MEXT) and a grant for research to promote the development of anti-AIDS pharmaceuticals from the Japan Health Sciences Foundation (to KK). ALM gratefully acknowledges BBSRC for financial support and with KK the Prime Ministers Initiative 2 (Connect) fund for collaborative twinning.

Appendix A. Supplementary data

Supplementary data associated with this article can be found, in the online version, at doi:10.1016/j.bbabio.2009.12.021.

References

[1] WHO, Control and surveillance of African trypanosomiasis, Report of a WHO Expert Committee, World Health Organ Tech Rep Ser, vol. 881, 1998, pp. 1–114, I–VI.
[2] C.E. Clayton, P. Michels, Metabolic compartmentation in African trypanosomes, Parasitol. Today 12 (1996) 465–471.
[3] F.R. Opperdoes, P. Borst, S. Bakker, W. Leene, Localization of glycerol-3-phosphate oxidase in the mitochondrion and particulate NAD+-linked glycerol-3-phosphate dehydrogenase in the microbodies of the bloodstream form to *Trypanosoma brucei*, Eur. J. Biochem. 76 (1977) 29–39.
[4] A.B. Clarkson Jr., E.J. Bienen, G. Pollakis, R.W. Grady, Respiration of bloodstream forms of the parasite *Trypanosoma brucei brucei* is dependent on a plant-like alternative oxidase, J. Biol. Chem. 264 (1989) 17770–17776.
[5] M. Chaudhuri, R.D. Ott, G.C. Hill, Trypanosome alternative oxidase: from molecule to function, Trends Parasitol. 22 (2006) 484–491.
[6] C. Nihei, Y. Fukai, K. Kita, Trypanosome alternative oxidase as a target of chemotherapy, Biochim. Biophys. Acta 1587 (2002) 234–239.
[7] N. Minagawa, Y. Yabu, K. Kita, K. Nagai, N. Ohta, K. Meguro, S. Sakajo, A. Yoshimoto, An antibiotic, ascofuranone, specifically inhibits respiration and in vitro growth of long slender bloodstream forms of *Trypanosoma brucei brucei*, Mol. Biochem. Parasitol. 84 (1997) 271–280.
[8] Y. Yabu, A. Yoshida, T. Suzuki, C. Nihei, K. Kawai, N. Minagawa, T. Hosokawa, K. Nagai, K. Kita, N. Ohta, The efficacy of ascofuranone in a consecutive treatment on *Trypanosoma brucei brucei* in mice, Parasitol. Int. 52 (2003) 155–164.
[9] Y. Yabu, T. Suzuki, C. Nihei, N. Minagawa, T. Hosokawa, K. Nagai, K. Kita, N. Ohta, Chemotherapeutic efficacy of ascofuranone in *Trypanosoma vivax*-infected mice without glycerol, Parasitol. Int. 55 (2006) 39–43.
[10] M. Chaudhuri, W. Ajayi, S. Temple, G.C. Hill, Identification and partial purification of a stage-specific 33 kDa mitochondrial protein as the alternative oxidase of the *Trypanosoma brucei brucei* bloodstream trypomastigotes, J. Eukaryot. Microbiol. 42 (1995) 467–472.
[11] A.L. Moore, J.N. Siedow, The regulation and nature of the cyanide-resistant alternative oxidase of plant mitochondria, Biochim. Biophys. Acta 1059 (1991) 121–140.
[12] A.L. Moore, M.S. Albury, Further insights into the structure of the alternative oxidase: from plants to parasites, Biochem. Soc. Trans. 36 (2008) 1022–1026.
[13] J.N. Siedow, A.L. Umbach, The mitochondrial cyanide-resistant oxidase: structural conservation amid regulatory diversity, Biochim. Biophys. Acta 1459 (2000) 432–439.
[14] T. Joseph-Horne, D.W. Hollomon, P.M. Wood, Fungal respiration: a fusion of standard and alternative components, Biochim. Biophys. Acta 1504 (2001) 179–195.
[15] A. McDonald, G. Vanlerberghe, Branched mitochondrial electron transport in the Animalia: presence of alternative oxidase in several animal phyla, IUBMB Life 56 (2004) 333–341.
[16] A.E. McDonald, G.C. Vanlerberghe, Alternative oxidase and plastoquinol terminal oxidase in marine prokaryotes of the Sargasso Sea, Gene 349 (2005) 15–24.
[17] A.E. McDonald, G.C. Vanlerberghe, J.F. Staples, Alternative oxidase in animals: unique characteristics and taxonomic distribution, J. Exp. Biol. 212 (2009) 2627–2634.
[18] D.A. Berthold, M.E. Andersson, P. Nordlund, New insight into the structure and function of the alternative oxidase, Biochim. Biophys. Acta 1460 (2000) 241–254.
[19] C. Affourtit, M.S. Albury, P.G. Crichton, A.L. Moore, Exploring the molecular nature of alternative oxidase regulation and catalysis, FEBS Lett. 510 (2002) 121–126.
[20] D.P. Maxwell, Y. Wang, L. McIntosh, The alternative oxidase lowers mitochondrial reactive oxygen production in plant cells, Proc. Natl. Acad. Sci. U. S. A. 96 (1999) 8271–8276.
[21] A.L. Moore, M.S. Albury, P.G. Crichton, C. Affourtit, Function of the alternative oxidase: is it still a scavenger? Trends Plant Sci. 7 (2002) 478–481.
[22] S. Mackenzie, L. McIntosh, Higher plant mitochondria, Plant Cell 11 (1999) 571–586.
[23] J.N. Siedow, A.L. Umbach, A.L. Moore, The active site of the cyanide-resistant oxidase from plant mitochondria contains a binuclear iron center, FEBS Lett. 362 (1995) 10–14.
[24] M.E. Andersson, P. Nordlund, A revised model of the active site of alternative oxidase, FEBS Lett. 449 (1999) 17–22.
[25] M.S. Albury, C. Affourtit, A.L. Moore, A highly conserved glutamate residue (Glu-270) is essential for plant alternative oxidase activity, J. Biol. Chem. 273 (1998) 30301–30305.
[26] M. Chaudhuri, W. Ajayi, G.C. Hill, Biochemical and molecular properties of the *Trypanosoma brucei* alternative oxidase, Mol. Biochem. Parasitol. 95 (1998) 53–68.
[27] W.U. Ajayi, M. Chaudhuri, G.C. Hill, Site-directed mutagenesis reveals the essentiality of the conserved residues in the putative diiron active site of the trypanosome alternative oxidase, J. Biol. Chem. 277 (2002) 8187–8193.
[28] M.S. Albury, C. Affourtit, P.G. Crichton, A.L. Moore, Structure of the plant alternative oxidase. Site-directed mutagenesis provides new information on the active site and membrane topology, J. Biol. Chem. 277 (2002) 1190–1194.
[29] K. Nakamura, K. Sakamoto, Y. Kido, Y. Fujimoto, T. Suzuki, M. Suzuki, Y. Yabu, N. Ohta, A. Tsuda, M. Onuma, K. Kita, Mutational analysis of the *Trypanosoma vivax* alternative oxidase: the $E(X)_6Y$ motif is conserved in both mitochondrial alternative oxidase and plastid terminal oxidase and is indispensable for enzyme activity, Biochem. Biophys. Res. Commun. 334 (2005) 593–600.
[30] D.A. Berthold, N. Voevodskaya, P. Stenmark, A. Graslund, P. Nordlund, EPR studies of the mitochondrial alternative oxidase. Evidence for a diiron carboxylate center, J. Biol. Chem. 277 (2002) 43608–43614.
[31] A.L. Moore, J.E. Carre, C. Affourtit, M.S. Albury, P.G. Crichton, K. Kita, P. Heathcote, Compelling EPR evidence that the alternative oxidase is a diiron carboxylate protein, Biochim. Biophys. Acta 1777 (2008) 327–330.
[32] A. Maréchal, Y. Kido, K. Kita, A.L. Moore, P.R. Rich, Identification of three redox states of recombinant *Trypanosoma brucei* alternative oxidase by FTIR spectroscopy and electrochemistry, J. Biol. Chem. 284 (2009) 31827–31833.
[33] Y. Fukai, H. Amino, H. Hirawake, Y. Yabu, N. Ohta, N. Minagawa, S. Sakajo, A. Yoshimoto, K. Nagai, S. Takamiya, S. Kojima, K. Kita, Functional expression of the ascofuranone-sensitive *Trypanosoma brucei brucei* alternative oxidase in the cytoplasmic membrane of *Escherichia coli*, Comp. Biochem. Physiol. C Pharmacol. Toxicol. Endocrinol. 124 (1999) 141–148.
[34] K. Kita, K. Konishi, Y. Anraku, Terminal oxidases of *Escherichia coli* aerobic respiratory chain. I. Purification and properties of cytochrome b_{562}–*o* complex from cells in the early exponential phase of aerobic growth, J. Biol. Chem. 259 (1984) 3368–3374.
[35] K. Kita, K. Konishi, Y. Anraku, Terminal oxidases of *Escherichia coli* aerobic respiratory chain. II. Purification and properties of cytochrome b_{558}–*d* complex from cells grown with limited oxygen and evidence of branched electron-carrying systems, J. Biol. Chem. 259 (1984) 3375–3381.
[36] C. Nihei, Y. Fukai, K. Kawai, A. Osanai, Y. Yabu, T. Suzuki, N. Ohta, N. Minagawa, K. Nagai, K. Kita, Purification of active recombinant trypanosome alternative oxidase, FEBS Lett. 538 (2003) 35–40.
[37] O. Maglio, F. Nastri, V. Pavone, A. Lombardi, W.F. DeGrado, Preorganization of molecular binding sites in designed diiron proteins, Proc. Natl. Acad. Sci. U. S. A. 100 (2003) 3772–3777.
[38] M.P. Hendrich, E. Munck, B.G. Fox, J.D. Lipscomb, Integer-spin Epr studies of the fully reduced methane monooxygenase hydroxylase component, J. Am. Chem. Soc. 112 (1990) 5861–5865.
[39] W.A. van den Berg, A.A. Stevens, M.F. Verhagen, W.M. van Dongen, W.R. Hagen, Overproduction of the prismane protein from *Desulfovibrio desulfuricans* ATCC 27774 in *Desulfovibrio vulgaris* (Hildenborough) and EPR spectroscopy of the [6Fe–6S] cluster in different redox states, Biochim. Biophys. Acta 1206 (1994) 240–246.
[40] M. Hoefnagel, P.R. Rich, Q. Zhang, J.T. Wiskich, Substrate kinetics of the plant mitochondrial alternative oxidase and the effects of pyruvate, Plant Physiol. 115 (1997) 1145–1153.
[41] Y. Kido, T. Shiba, D.K. Inaoka, K. Sakamoto, T. Nara, T. Aoki, T. Honma, A. Tanaka, M. Inoue, S. Matsuoka, A. Moore, S. Harada, K. Kita, Crystallization and preliminary crystallographic analysis of cyanide-insensitive alternative oxidase from *Trypanosoma brucei brucei*, Acta. Crystallogr. Sect. F Struct. Biol. Cryst. Commun, doi:10.1107/S1744309109054062.
[42] H. Miyadera, H. Amino, A. Hiraishi, H. Taka, K. Murayama, H. Miyoshi, K. Sakamoto, N. Ishii, S. Hekimi, K. Kita, Altered quinone biosynthesis in the long-lived clk-1 mutants of *Caenorhabditis elegans*, J. Biol. Chem. 276 (2001) 7713–7716.
[43] P. Stenmark, J. Grunler, J. Mattsson, P.J. Sindelar, P. Nordlund, D.A. Berthold, A new member of the family of di-iron carboxylate proteins. Coq7 (clk-1), a membrane-bound hydroxylase involved in ubiquinone biosynthesis, J. Biol. Chem. 276 (2001) 33297–33300.
[44] D.A. Berthold, P. Stenmark, Membrane-bound diiron carboxylate proteins, Ann. Rev. Plant Biol. 54 (2003) 497–517.
[45] R. Fato, M. Cavazzoni, C. Castelluccio, G. Parenti Castelli, G. Palmer, M. Degli Esposti, G. Lenaz, Steady-state kinetics of ubiquinol–cytochrome *c* reductase in bovine heart submitochondrial particles: diffusional effects, Biochem. J. 290 (1993) 225–236 K.
[46] H. Witt, F. Malatesta, F. Nicoletti, M. Brunori, B. Ludwig, Tryptophan 121 of subunit II is the electron entry site to cytochrome-*c* oxidase in *Paracoccus denitrificans*. Involvement of a hydrophobic patch in the docking reaction, J. Biol. Chem. 273 (1998) 5132–5136.
[47] Sakamoto, H. Miyoshi, M. Ohshima, K. Kuwabara, K. Kano, T. Akagi, T. Mogi, H. Iwamura, Role of the isoprenyl tail of ubiquinone in reaction with respiratory enzymes: studies with bovine heart mitochondrial complex I and *Escherichia coli bo*-type ubiquinol oxidase, Biochemistry 37 (1998) 15106–15113.
[48] M.H.N. Hoefnagel, J.T. Wiskich, S.A. Madgwick, Z. Patterson, W. Oettmeier, P.R. Rich New, Inhibitors of the ubiquinol oxidase of higher plant mitochondria, Eur. J. Biochem. 233 (1995) 531–537.
[49] R.A. Alberty, G.G. Hammes, Application of the theory of diffusion-controlled reactions to enzyme kinetics, J. Phys. Chem. 62 (1958) 154–159.
[50] R. Clifton, A.H. Millar, J. Whelan, Alternative oxidases in Arabidopsis: a comparative analysis of differential expression in the gene family provides new insights into function of non-phosphorylating bypasses, Biochim. Biophys. Acta 1757 (2006) 730–741.
[51] A.M. Wagner, K. Krab, M.J. Wagner, A.L. Moore, Regulation of thermogenesis in flowering Araceae: the role of the alternative oxidase, Biochim. Biophys. Acta 1777 (2008) 993–1000.

[52] K. Sakamoto, H. Miyoshi, K. Takegami, T. Mogi, Y. Anraku, H. Iwamura, Probing substrate binding site of the *Escherichia coli* quinol oxidases using synthetic ubiquinol analogues, J. Biol. Chem. 271 (1996) 29897–29902.
[53] T. Suzuki, T. Hashimoto, Y. Yabu, Y. Kido, K. Sakamoto, C. Nihei, M. Hato, S. Suzuki, Y. Amano, K. Nagai, T. Hosokawa, N. Minagawa, N. Ohta, K. Kita, Direct evidence for cyanide-insensitive quinol oxidase (alternative oxidase) in apicomplexan parasite *Cryptosporidium parvum*: phylogenetic and therapeutic implications, Biochem. Biophys. Res. Commun. 313 (2004) 1044–1052.
[54] C.W. Roberts, F. Roberts, F.L. Henriquez, D. Akiyoshi, B.U. Samuel, T.A. Richards, W. Milhous, D. Kyle, L. McIntosh, G.C. Hill, M. Chaudhuri, S. Tzipori, R. McLeod, Evidence for mitochondrial-derived alternative oxidase in the apicomplexan parasite *Cryptosporidium parvum*: a potential anti-microbial agent target, Int. J. Parasitol. 34 (2004) 297–308.
[55] R. Walker Jr., L. Saha, G.C. Hill, M. Chaudhuri, The effect of over-expression of the alternative oxidase in the procyclic forms of *Trypanosoma brucei*, Mol. Biochem. Parasitol. 139 (2005) 153–162.
[56] E. Vassella, M. Probst, A. Schneider, E. Studer, C.K. Renggli, I. Roditi, Expression of a major surface protein of *Trypanosoma brucei* insect forms is controlled by the activity of mitochondrial enzymes, Mol. Biol. Cell 15 (2004) 3986–3993.
[57] A. Tsuda, W.H. Witola, K. Ohashi, M. Onuma, Expression of alternative oxidase inhibits programmed cell death-like phenomenon in bloodstream form of *Trypanosoma brucei rhodesiense*, Parasitol. Int. 54 (2005) 243–251.

Acta Crystallographica Section F
Structural Biology and Crystallization Communications
ISSN 1744-3091

Crystallization and preliminary crystallographic analysis of cyanide-insensitive alternative oxidase from *Trypanosoma brucei brucei*

Yasutoshi Kido,[a] Tomoo Shiba,[a] Daniel Ken Inaoka,[a] Kimitoshi Sakamoto,[a] Takeshi Nara,[b] Takashi Aoki,[b] Teruki Honma,[c] Akiko Tanaka,[c] Masayuki Inoue,[d] Shigeru Matsuoka,[d] Anthony Moore,[e] Shigeharu Harada[f]* and Kiyoshi Kita[a]*

[a]Department of Biomedical Chemistry, Graduate School of Medicine, The University of Tokyo, Tokyo 113-0033, Japan, [b]Department of Molecular and Cellular Parasitology, Juntendo University School of Medicine, Tokyo 113-8421, Japan, [c]Systems and Structural Biology Center, RIKEN, Tsurumi, Yokohama 230-0045, Japan, [d]Graduate School of Pharmaceutical Sciences, The University of Tokyo, Tokyo 113-0033, Japan, [e]Biochemistry and Biomedical Sciences, School of Life Sciences, University of Sussex, Falmer, Brighton, England, and [f]Department of Applied Biology, Graduate School of Science and Technology, Kyoto Institute of Technology, Kyoto 606-8585, Japan

Correspondence e-mail: harada@kit.ac.jp, kitak@m.u-tokyo.ac.jp

Received 6 September 2009
Accepted 15 December 2009

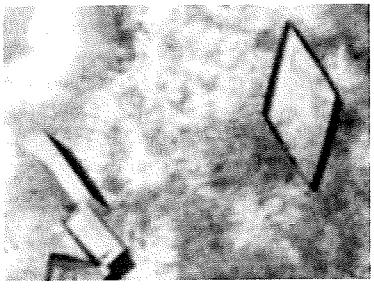

Cyanide-insensitive alternative oxidase (AOX) is a mitochondrial membrane protein and a non-proton-pumping ubiquinol oxidase that catalyzes the four-electron reduction of dioxygen to water. In the African trypanosomes, trypanosome alternative oxidase (TAO) functions as a cytochrome-independent terminal oxidase that is essential for survival in the mammalian host; hence, the enzyme is considered to be a promising drug target for the treatment of trypanosomiasis. In the present study, recombinant TAO (rTAO) overexpressed in haem-deficient *Escherichia coli* was purified and crystallized at 293 K by the hanging-drop vapour-diffusion method using polyethylene glycol 400 as a precipitant. X-ray diffraction data were collected at 100 K and were processed to 2.9 Å resolution with 93.1% completeness and an overall $R_{\rm merge}$ of 9.5%. The TAO crystals belonged to the orthorhombic space group $I222$ or $I2_12_12_1$, with unit-cell parameters $a = 63.11$, $b = 136.44$, $c = 223.06$ Å. Assuming the presence of two rTAO molecules in the asymmetric unit (2 × 38 kDa), the calculated Matthews coefficient ($V_{\rm M}$) was 3.2 Å^3 Da^{-1}, which corresponds to a solvent content of 61.0%. This is the first report of a crystal of the membrane-bound diiron proteins, which include AOXs.

1. Introduction

Cyanide-insensitive respiration in plants has been recognized since the 1920s (Moore & Siedow, 1991). Intensive biochemical studies have revealed that the mitochondrial membrane enzyme alternative oxidase (AOX) is responsible for cyanide-insensitive respiration (Moore & Siedow, 1991; Siedow & Umbach, 2000; Moore & Albury, 2008). AOX, which is cyanide-insensitive and sensitive to salicyl hydroxamic acid (SHAM), is a non-proton-pumping ubiquinol oxidase that catalyzes the four-electron reduction of dioxygen to water (Moore & Albury, 2008). AOX has been found in higher plants, algae, yeast, slime moulds, free-living amoebae, eubacteria and nematodes, as well as in protozoa, including trypanosomes (McDonald *et al.*, 2009).

Trypanosoma brucei, which causes African sleeping sickness in humans and nagana in livestock, which are serious health and economic problems in sub-Saharan Africa (World Health Organization, 2006), is known to show cyanide-insensitive respiration (Opperdoes *et al.*, 1977; Chaudhuri *et al.*, 2006). In the African trypanosomes, trypanosome alternative oxidase (TAO) functions in cyanide-insensitive respiration as a cytochrome-independent terminal oxidase (Clarkson *et al.*, 1989) that is essential for survival in the mammalian host (Clayton & Michels, 1996; Chaudhuri *et al.*, 2006).

TAO is thought to be a good target for antitrypanosomal drugs because mammalian hosts do not possess this protein (Nihei *et al.*, 2002; Chaudhuri *et al.*, 2006). Indeed, we found that ascofuranone, which is isolated from the pathogenic fungus *Ascochyta visiae*, specifically inhibits the quinol oxidase activity of TAO (Minagawa *et al.*, 1997) and rapidly kills the parasites. In addition, we have confirmed the chemotherapeutic efficacy of ascofuranone *in vivo* (Yabu *et al.*, 2003, 2006).

Although TAO and other alternative oxidases (AOXs) contain diiron-binding motifs (E*XX*H) in their amino-acid sequences, their three-dimensional structures have not yet been elucidated (Berthold

& Stenmark, 2003; Moore & Albury, 2008). The high-resolution structure of TAO will undoubtedly have considerable implications with respect to their physicochemical mechanism, enzyme reaction and structure–function relationship, including the interaction between the enzyme and ascofuranone, which may lead to the rational design of more potent and safer antitrypanosomal drugs. Here, we describe the crystallization and preliminary crystallographic analysis of TAO.

2. Materials and methods

2.1. Preparation of rTAO

To construct the host strain FN102 for the expression of rTAO, the Δ*hemA*::Km^R mutation was introduced into *Escherichia coli* strain BL21 (DE3) by P1 transduction as described in a previous study (Nihei *et al.*, 2003). The strain FN102/pTbAO (Nihei *et al.*, 2003) carrying the cDNA for *T. brucei brucei* TAO was precultured at 310 K in 100 ml LB medium (containing 10 mg ampicillin, 5 mg kanamycin and 5 mg 5-aminolevulinic acid) for 4–6 h. The precultured cells were grown aerobically at 303 K in 10 l S-medium [100 g tryptone peptone, 50 g yeast extract, 50 g casamino acids, 104 g K_2HPO_4, 30 g KH_2PO_4, 7.5 g trisodium citrate.$2H_2O$, 25 g $(NH_4)_2SO_4$, 0.5 g $MgSO_4.7H_2O$, 0.25 g $FeSO_4.7H_2O$, 0.25 g $FeCl_3$, 20 g glucose and 0.1 g carbenicillin]. The culture was started at an OD_{600} of 0.01 and expression of His_6-tagged rTAO was induced by the addition of isopropyl β-D-1-thiogalactopyranoside (IPTG; 25 μ*M*) when the OD_{600} reached 0.1. The cells were harvested 8–10 h after induction (about 40 g wet weight). The cells were then resuspended in 200 ml 50 m*M* Tris–HCl pH 7.5 containing 20%(*w*/*w*) sucrose, 0.1 m*M* phenylmethanesulfonylfluoride and protease inhibitor cocktail (Sigma) and broken using a French pressure cell at 200 MPa (Ohtake, Tokyo). Unbroken cells were removed as a pellet by centrifugation at 8000*g* for 10 min (Hitachi 21G). The supernatant (35 ml) was loaded onto 35 ml 50 m*M* Tris–HCl pH 7.5 containing 40%(*w*/*w*) sucrose and ultracentrifuged at 200 000*g* for 1 h at 277 K (Hitachi 85H); the fraction of inner membranes buoyant on the 40%(*w*/*w*) sucrose layer was recovered. The inner-membrane pellet was separated by further ultracentrifugation at 200 000*g* for 1 h (Hitachi 85H) and was resuspended in 30 ml 50 m*M* Tris–HCl pH 7.5 containing 20%(*w*/*w*) sucrose. To solubilize rTAO from the membranes, the membrane suspension (35 ml) was diluted with buffer [50 m*M* Tris–HCl, 200 m*M* $MgSO_4$, 20%(*v*/*v*) glycerol pH 7.3] at 277 K to give a 6 mg ml^{-1} solution and 14%(*w*/*v*) *n*-octyl β-D-glucopyranoside (OG) was added to a final concentration of 1.4%(*w*/*v*). The solution was immediately ultracentrifuged at 200 000*g* for 1 h at 277 K to recover the supernatant containing the solubilized rTAO.

Cobalt-affinity chromatography was performed by a hybrid batch/column procedure using the manufacturer's instructions as stated below. 10 ml BD TALON Metal Affinity Resin (BD Bioscience) equilibrated in a batch format with 100 ml equilibration buffer [20 m*M* Tris–HCl, 1.4%(*w*/*v*) OG, 100 m*M* $MgSO_4$, 20%(*v*/*v*) glycerol pH 7.3] was mixed with 20 ml of the OG extract for 20 min at 277 K. The resin was washed twice with 100 ml of the first wash buffer [20 m*M* Tris–HCl, 20 m*M* imidazole, 0.042%(*w*/*v*) *n*-dodecyl β-D-maltopyranoside (DM), 50 m*M* $MgSO_4$, 20%(*v*/*v*) glycerol pH 7.3] and then transferred to a column for additional washing with 20 ml of the second wash buffer [20 m*M* Tris–HCl, 165 m*M* imidazole, 0.042%(*w*/*v*) DM, 50 m*M* $MgSO_4$, 20%(*v*/*v*) glycerol pH 7.3; flow rate 1 ml min^{-1}]. After washing, rTAO was eluted with elution buffer [20 m*M* Tris–HCl, 200 m*M* imidazole, 0.042%(*w*/*v*) DM, 50 m*M* $MgSO_4$, 60 m*M* NaCl, 20%(*v*/*v*) glycerol pH 7.3; flow rate 1 ml min^{-1}] and the fractions containing rTAO as judged by activity measurements and SDS–PAGE were pooled (Kido *et al.*, 2010).

The fused N-terminal His_6 tag was removed from the purified rTAO using biotinylated thrombin and the tag-free rTAO was separated using streptavidin agarose (Biotinylated Thrombin Cleavage Capture Kit, Novagen) according to the manufacturer's instructions. Incubation with 10 U thrombin for 16 h at 293 K was required for the complete cleavage of 10 mg protein.

The molecular weight of the enzyme in solution was estimated by gel-filtration chromatography using a HiLoad 16/60 Superdex 200 pg column (GE Healthcare). Elution was carried out at a flow rate of 0.3 ml min^{-1} using 50 m*M* Tris–HCl pH 7.4, 0.1 *M* NaCl, 0.042%(*w*/*v*) DM and 20%(*v*/*v*) glycerol.

2.2. Crystallization and X-ray data collection

The purified rTAO was concentrated to 5 mg ml^{-1} in 20 m*M* Tris–HCl, 0.042%(*w*/*v*) DM, 50 m*M* $MgSO_4$, 20%(*v*/*v*) glycerol pH 7.3 using an Amicon Ultra centrifugal filter device (Millipore, 30 kDa molecular-weight cutoff) and used for initial screening of crystallization conditions. Crystallization was performed by the sitting-drop vapour-diffusion technique in 96-well Corning CrystalEX microplates with a conical flat bottom (Hampton Research). In the screening, 0.5 μl rTAO solution was mixed with an equal volume of reservoir solution and the droplet was equilibrated against 100 μl reservoir solution at 277 and 293 K. Commercially available screening kits purchased from Hampton Research (Crystal Screen, Crystal Screen II, Crystal Screen Lite, SaltRx and MembFac), Emerald BioStructures (Wizard I, Wizard II, Cryo I and Cryo II) and Fluidigm (OptiMax-5 Membrane), together with homemade grid-screen reagents containing 100 m*M* buffer (pH 5.0–9.0), 10–40%(*w*/*v*) polyethylene glycol (PEG 400, PEG 1000, PEG 3350, PEG 6000 and PEG 10 000) and 200 m*M* salts (NaCl and KCl), were used as reservoir solutions. However, crystals of rTAO did not appear.

Subsequently, screening was carried out at 277 K using various detergents (DM, OG, *n*-decyl β-D-maltopyranoside, *n*-octyl β-D-maltopyranoside, *n*-nonanoyl *N*-methyl-D-glucamine, octaethylene glycol monododecylether, tetraethylene glycol monooctylether and hexaethylene glycol monodecylether). rTAO samples dissolved in different detergents were subjected to free-interface diffusion in a TOPAZ 8.96 Screening Tip against reservoir solutions purchased from TOPAZ (OptiMax-1, OptiMax-2, OptiMax-3, OptiMax-4 PEG and OptiMax-5 Membrane) using a Fluidigm TOPAZ system (Segelke, 2005). When OG was used as a detergent, several reservoir solutions containing low-molecular-weight PEGs as precipitants gave tiny crystals. The conditions were further optimized by varying the PEG (PEG 200, PEG 400 and PEG 1000) concentration (10–40%), the buffer pH (6.0–8.0), the salt type (48 salts found in PEG/Ion Screen kit from Hampton Research) and the temperature (277 and 293 K) using the sitting-drop vapour-diffusion method. However, crystals larger than 30 μm could not be obtained and moreover they only diffracted X-rays to 7 Å resolution at most.

Next, the effects of additive detergents on crystal growth and X-ray diffraction were examined using reservoir solutions [25–40%(*w*/*v*) PEG 400, 100 m*M* imidazole buffer pH 6.2–7.8 and 200 m*M* potassium formate] supplemented with 0.1–0.5%(*w*/*v*) additive detergents. A dramatic improvement in crystal size was achieved using tetraethylene glycol monooctylether (C8E4) and the conditions, including the concentration of C8E4, were finally optimized.

Currently, crystals with average dimensions of approximately 0.1 × 0.07 × 0.03 mm can be reproducibly obtained at 293 K from reservoir solution consisting of 28–34%(*w*/*v*) PEG 400, 100 m*M*

imidazole buffer pH 7.4, 500 m*M* potassium formate and 0.4%(*w*/*v*) C8E4 using rTAO dissolved in 20 m*M* Tris–HCl pH 7.3, 0.8%(*w*/*v*) OG, 20 m*M* $MgSO_4$ and 20%(*v*/*v*) glycerol.

X-ray diffraction experiments were performed using synchrotron radiation on BL44XU and BL41XU at SPring-8 (Harima, Japan), BL5A and BL17A at Photon Factory and NW12A at Photon Factory Advanced Ring (Tsukuba, Japan). A crystal mounted in a nylon loop was frozen by rapidly submerging it in liquid nitrogen and X-ray diffraction patterns were recorded at 100 K. The best crystals diffracted X-rays to better than 3.0 Å resolution and a total of 180 images were recorded with an oscillation angle of 1°, an exposure time of 5 s per image and a crystal-to-detector distance of 280 mm. The data were processed and scaled using the *HKL*-2000 software package (Otwinowski & Minor, 1997).

3. Results and discussion

His_6-tagged rTAO was solubilized from inner membranes using OG and was purified by cobalt-affinity chromatography in the presence of DM. After removal of the fused N-terminal His_6 tag, about 10 mg of enzyme was obtained from a 10 l culture. The purified rTAO, consisting of 329 amino-acid residues (38 kDa), was >95% pure as estimated by SDS–PAGE (Fig. 1) and its molecular weight in solution was estimated to be 110 kDa by gel-filtration chromatography. As rTAO was prepared as a water-soluble rTAO–DM complex, the complex is probably composed of a homodimer of rTAO with DM molecules bound to the hydrophobic surface of the homodimer. A homodimeric structure of TAO has also been suggested by Chaudhuri *et al.* (2005). The molecular weight of the rTAO–OG complex could not be estimated because elution of rTAO from the gel-filtration column was only successful in the presence of DM as a detergent.

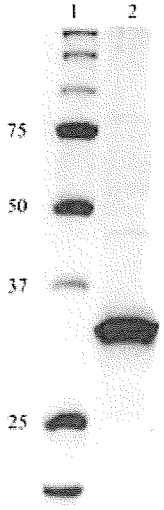

Figure 1
12.5% SDS–PAGE of rTAO with Coomassie Brilliant Blue R-250 staining. Lane 1, molecular-weight markers (kDa); lane 2, rTAO purified by affinity chromatography using BD TALON Metal Affinity Resin.

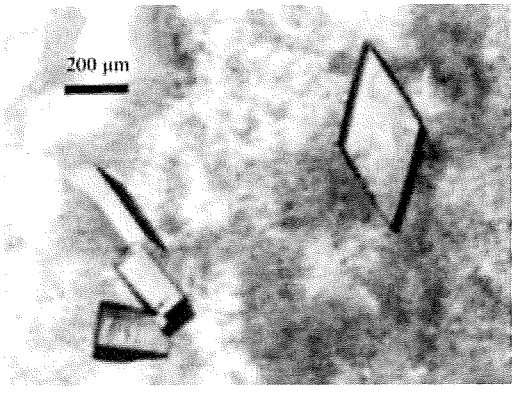

Figure 2
Rhombic plate-shaped crystals of rTAO obtained by the sitting-drop vapour-diffusion method using PEG 400 as a precipitant.

Table 1
Diffraction data statistics.

Values in parentheses are for the outermost resolution shell.

Space group	$I222$ or $I2_12_12_1$
Unit-cell parameters (Å)	a = 63.11, b = 136.44, c = 223.06
Beamline	SPring-8 BL41XU
Wavelength (Å)	1.000
Temperature (K)	100
Resolution (Å)	50.0– 2.90 (2.95–2.90)
Total reflections	135535
Unique reflections	21720
Completeness (%)	93.1 (63.2)
$R_{merge}(I)$† (%)	9.5 (57.3)
$\langle I/\sigma(I)\rangle$	9.8 (1.7)

† $R_{merge}(I) = \sum_{hkl}\sum_i |I_i(hkl) - \langle I(hkl)\rangle| / \sum_{hkl}\sum_i I_i(hkl)$, where $I_i(hkl)$ is the ith measurement of reflection hkl.

After extensive screening and optimization of crystallization conditions, crystals with average dimensions of approximately 0.1 × 0.07 × 0.03 mm could be obtained within 10 d at 293 K using rTAO dissolved in 20 m*M* Tris–HCl pH 7.3, 0.8%(*w*/*v*) OG, 20 m*M* $MgSO_4$ and 20%(*v*/*v*) glycerol with a reservoir solution containing 28–34%(*w*/*v*) PEG 400, 100 m*M* imidazole buffer pH 7.4, 100 m*M* potassium formate and 0.4%(*w*/*v*) C8E4 (Fig. 2).

Analyses of the symmetry and systematic absences in the recorded diffraction patterns indicated that the crystals belonged to the orthorhombic space group $I222$ or $I2_12_12_1$, with unit-cell parameters a = 63.11, b = 136.44, c = 223.06 Å. Assuming the presence of two rTAO molecules in the asymmetric unit (2 × 38 kDa), the calculated Matthews coefficient (V_M) is 3.2 $Å^3\ Da^{-1}$, which corresponds to a solvent content of 61.0%. If the molecular weight of the rTAO–OG complex is presumed to be comparable to that of the rTAO–DM complex, the presence of one molecule of the rTAO–OG complex in the asymmetric unit gives a V_M value of 2.2 $Å^3\ Da^{-1}$ and a solvent content of 44.1%. A data set to 2.9 Å resolution (21 720 unique reflections) was obtained after merging 135 535 reflections recorded on 180 images, with 93.1% completeness and an overall R_{merge} of 9.5%. Statistics of data collection and processing are shown in Table 1. Currently, data collection for phasing using the anomalous dispersion effect of iron is in progress. This is the first report of the crystallization of membrane-bound diiron proteins, which include AOXs.

We thank all staff members of beamlines BL44XU and BL41XU at SPring-8, BL5A and BL17A at Photon Factory and NW12 at Photon Factory Advanced Ring for their help with X-ray diffraction data collection. This work was supported in part by grant-in-aid for Young Scientists (B) 21790402 (to YK), Creative Scientific Research Grant 18GS0314 (to KK), grant-in-aid for Scientific Research on Priority Areas 18073004 (to KK) from the Japanese Society for the Promotion of Science and the Targeted Proteins Research Program (to KK) of the Japanese Ministry of Education, Science, Culture, Sports and Technology (MEXT). ALM gratefully acknowledges the BBSRC for

financial support and, together with KK, the Prime Minister's Initiative 2 (Connect) fund for collaborative twinning.

References

Berthold, D. A. & Stenmark, P. (2003). *Annu. Rev. Plant Biol.* **54**, 497–517.
Chaudhuri, M., Ott, R. D. & Hill, G. C. (2006). *Trends Parasitol.* **22**, 484–491.
Chaudhuri, M., Ott, R. D., Saha, L., Williams, S. & Hill, G. C. (2005). *Parasitol. Res.* **96**, 178–183.
Clarkson, A. B. Jr, Bienen, E. J., Pollakis, G. & Grady, R. W. (1989). *J. Biol. Chem.* **264**, 17770–17776.
Clayton, C. E. & Michels, P. (1996). *Parasitol. Today*, **12**, 465–471.
Kido, Y., Sakamoto, K., Nakamura, K., Harada, M., Suzuki, T., Yabu, Y., Saimoto, H., Yamakura, F., Ohmori, D., Moore, A., Harada, S. & Kita, K., (2010). *Biochim. Biophys. Acta*, doi:10.1016/j.bbabio.2009.12.021.
McDonald, A. E., Vanlerberghe, G. C. & Staples, J. F. (2009). *J. Exp. Biol.* **212**, 2627–2634.
Minagawa, N., Yabu, Y., Kita, K., Nagai, K., Ohta, N., Meguro, K., Sakajo, S. & Yoshimoto, A. (1997). *Mol. Biochem. Parasitol.* **84**, 271–280.
Moore, A. L. & Albury, M. S. (2008). *Biochem. Soc. Trans.* **36**, 1022–1026.
Moore, A. L. & Siedow, J. N. (1991). *Biochim. Biophys. Acta*, **1059**, 121–140.
Nihei, C., Fukai, Y., Kawai, K., Osanai, A., Yabu, Y., Suzuki, T., Ohta, N., Minagawa, N., Nagai, K. & Kita, K. (2003). *FEBS Lett.* **538**, 35–40.
Nihei, C., Fukai, Y. & Kita, K. (2002). *Biochim. Biophys. Acta*, **1587**, 234–239.
Opperdoes, F. R., Borst, P., Bakker, S. & Leene, W. (1977). *Eur. J. Biochem.* **76**, 29–39.
Otwinowski, Z. & Minor, W. (1997). *Methods Enzymol.* **276**, 307–326.
Segelke, B. (2005). *Expert Rev. Proteomics*, **2**, 165–172.
Siedow, J. N. & Umbach, A. L. (2000). *Biochim. Biophys. Acta*, **1459**, 432–439.
World Health Organization (2006). *Wkly Epidemiol. Rec.* **81**, 71–80.
Yabu, Y., Suzuki, T., Nihei, C., Minagawa, N., Hosokawa, T., Nagai, K., Kita, K. & Ohta, N. (2006). *Parasitol. Int.* **55**, 39–43.
Yabu, Y., Yoshida, A., Suzuki, T., Nihei, C., Kawai, K., Minagawa, N., Hosokawa, T., Nagai, K., Kita, K. & Ohta, N. (2003). *Parasitol. Int.* **52**, 155–164.

J|A|C|S
COMMUNICATIONS

Published on Web 12/23/2007

Paramagnetic Relaxation-Based ^{19}F MRI Probe To Detect Protease Activity

Shin Mizukami,† Rika Takikawa,† Fuminori Sugihara,‡ Yuichiro Hori,† Hidehito Tochio,§ Markus Wälchli,⊥ Masahiro Shirakawa,*,§,¶ and Kazuya Kikuchi*,†

Division of Advanced Science and Biotechnology, Graduate School of Engineering, Osaka University, Osaka 565-0871, Japan, International Graduate School of Arts and Sciences, Yokohama City University, Kanagawa 230-0045, Japan, Department of Molecular Engineering, Graduate School of Engineering, Kyoto University, Kyoto 615-8510, Japan, Bruker BioSpin K.K., Ibaraki 305-0051, Japan, and CREST, Japan Science and Technology Corporation, Saitama 332-0012, Japan

Received September 12, 2007; E-mail: kkikuchi@mls.eng.osaka-u.ac.jp; shirakawa@moleng.kyoto-u.ac.jp

Real-time imaging of enzyme activities in vivo offers valuable information in understanding living systems and in developing medicine for various types of diseases. Currently, a variety of fluorescent probes for detecting enzyme activities are generally used for their high-sensitivity characteristics. However, general fluorescence imaging methods are not suitable for in vivo studies because visible fluorescence scarcely transmits through animal bodies. Although near-infrared fluorophores are useful for in vivo imaging for tissue surfaces, they cannot be applied to the deep section of the organ. On the other hand, magnetic resonance imaging (MRI) is known as an imaging technique adequate for in vivo studies.

^1H is a highly NMR-sensitive nuclide and abundant in living bodies. Thus, ^1H MRI is used as a powerful diagnostic imaging technique for identifying many human pathologies or medical conditions. Paramagnetic contrast agents such as several types of Gd complexes are in clinical use for their abilities to enhance the signal intensity by shortening the longitudinal relaxation time (T_1) of water protons. Presently, many scientists are interested in modifying the structures of the contrast agents to be functional in molecular imaging of biomolecules.[1] MRI probes for pH,[2] metal ions,[3] enzyme activities,[4] and so on have been developed. However, ^1H MRI often suffers from interference or low contrast due to the background signals from intrinsic ^1H, which hamper interpretation of the resultant images. Therefore, non-proton MRI is currently drawing a fair amount of attention.

One of the most promising nuclides for MRI is ^{19}F.[5] This nuclide has a high gyromagnetic ratio (γ) of 40.05 MHz/T and a 100% natural isotopic abundance ratio. Thus, the NMR sensitivity of ^{19}F is 0.83 relative to ^1H. Conveniently, due to their close γ values, ^{19}F NMR can be measured with most ^1H NMR instruments by appropriately tuning the RF coils. In our bodies, ^{19}F atoms are concentrated in the form of solid salts mostly in bones and teeth. Thus, the transverse relaxation time (T_2) of the intrinsic ^{19}F is extremely shortened,[6] and the MRI signal is hardly detectable. When ^{19}F-containing compounds are treated in human or animals, only the extrinsic ^{19}F MRI signals can be monitored without interference from background signals. For these above reasons, functional probes for ^{19}F MRI are very attractive for in vivo molecular imaging.

Known ^{19}F MRI probes are roughly categorized into two groups; one is the group of ^{19}F-containing compounds which accumulate in specific sites. Higuchi and co-workers synthesized a ^{19}F-containing thioflavin derivative that accumulates in amyloid β (Aβ) aggregates and visualized Aβ plaques in living animals by ^{19}F MRI.[7]

Scheme 1. Design Principle of ^{19}F MRI Probe Detecting a Protease Activity

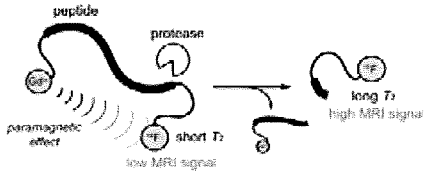

Another class of ^{19}F MRI probes is active agents.[5] They undergo chemical modification by the target molecules and then change their NMR parameters. Mason and co-workers have developed ^{19}F MRI probes detecting reporter enzyme activities by the chemical shift change.[8] These probes are hydrolyzed by the reporter enzyme and change the ^{19}F chemical shift. Although this approach is promising, this is highly dependent on the magnitude of chemical shift changes coupled with the target reaction, where sometimes the ranges of the chemical shift changes are limited. We here propose a novel design strategy for ^{19}F MRI probes in detecting protease activity.

We constructed a design principle whereby the intramolecular paramagnetic effect for T_2 of the ^{19}F NMR signal can be modulated by protease activities. T_2 is an important contrast factor for MRI, as the apparent intensity of the MRI signal directly depends on T_2 values. Generally, paramagnetic metal ions such as Fe^{3+}, Gd^{3+}, or the paramagnetic molecules such as O_2 shorten the T_2 of samples by paramagnetic relaxation enhancement (PRE).[9] In particular, Gd^{3+} has a very strong relaxivity (T_2-shortening activity) because of its large electron spin quantum number. When ^{19}F nuclei and a Gd^{3+} ion are attached to a short peptide, the ^{19}F nuclei exhibit a strong paramagnetic effect from the Gd^{3+}. Thus, the T_2 of the compound in the ^{19}F NMR would be shortened, and the MRI signal would be attenuated. If the peptide has a substrate sequence which can be cleaved by a certain protease, incubation of the compound with the protease should induce the extension of the T_2 and the enhancement of the ^{19}F MRI signal (Scheme 1).

According to the above strategy, we synthesized a ^{19}F MRI probe, Gd-DOTA-DEVD-Tfb, for detecting caspase-3 activity (Figure 1). Caspase-3 is a marker enzyme of apoptosis and is used in the evaluation of anticancer agents inducing apoptosis of tumor cells. The probe consists mainly of three parts, which are a Gd^{3+} complex, an enzyme substrate peptide, and a ^{19}F-containing group. The peptide sequence is DEVD because caspase-3 selectively cleaves the C-terminal peptide bond of the sequence DXXD (X: optional).[10] A macrocyclic metal ligand, DOTA, was attached via a β-alanine linker with the N-terminus of ^{19}F-containing peptide DEVD-Tfb, which was synthesized by Fmoc solid-phase peptide synthesis. The ligand-conjugated peptide, DOTA-DEVD-Tfb, was complexed with Gd^{3+} ion and purified with a reversed-phase HPLC to yield Gd-

† Osaka University.
‡ Yokohama City University.
§ Kyoto University.
⊥ Bruker BioSpin K.K.
¶ CREST, JST.

10.1021/ja077058z CCC: $40.75

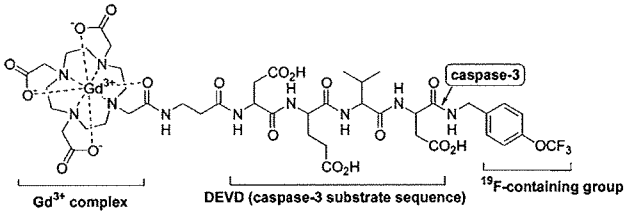

Figure 1. Structure of Gd-DOTA-DEVD-Tfb.

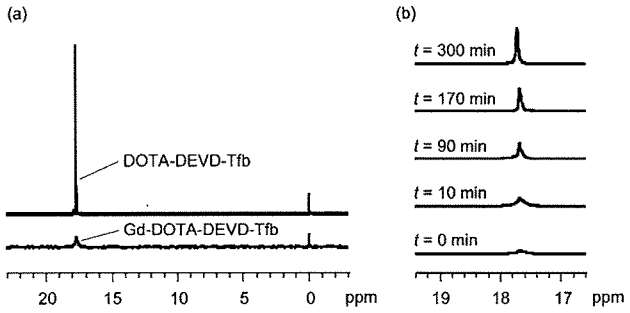

Figure 2. (a) ^{19}F NMR spectra of DOTA-DEVD-Tfb (1 mM) and Gd-DOTA-DEVD-Tfb (1 mM). Sodium trifluoroacetate was added as an internal standard (0 ppm). (b) Time-dependent ^{19}F NMR spectral change of Gd-DOTA-DEVD-Tfb with caspase-3 at 37 °C.

DOTA-DEVD-Tfb. The probe structure was identified with ESI-TOF MS, and its purity was confirmed by HPLC and ^{19}F NMR.

Next, we measured the ^{19}F T_1 and T_2 values of the probe free from and in complex with Gd^{3+}. The T_1 and T_2 of DOTA-DEVD-Tfb (1 mM) were 1.910 and 0.326 s, respectively. In contrast, the values of Gd-DOTA-DEVD-Tfb could not be measured, due to markedly shorter relaxation times and the low signal intensity of the ^{19}F resonance. This result indicates that the ^{19}F nucleus of Gd-DOTA-DEVD-Tfb undergoes strong PRE by Gd^{3+}. This effect was explicitly shown in the one-dimensional ^{19}F NMR spectrum, in which the peak intensity of Gd-DOTA-DEVD-Tfb was largely decreased with broadening as compared with that of DOTA-DEVD-Tfb (Figure 2a). When we treated the Gd-DOTA-DEVD-Tfb with caspase-3 at 37 °C, the ^{19}F NMR peak became sharper and higher in a time-dependent manner (Figure 2b). This indicated the intramolecular paramagnetic effect from Gd^{3+} to ^{19}F was cancelled by the cleavage of the probe. The T_1 and T_2 of the 1 mM cleaved product were extended to 0.122 and 0.032 s, respectively. These values are still shorter than those of DOTA-DEVD-Tfb. An additional experiment suggests that this is because of the intermolecular PRE by the Gd^{3+} complex (Figure S4 in Supporting Information).

Finally, an attempt was made to visualize caspase-3 activity using a ^{19}F MRI phantom to verify the practical applicability of this probe and its sensing principle. As was expected, Gd-DOTA-DEVD-Tfb showed no signal on the ^{19}F MRI phantom image. Time course of the density-weighted ^{19}F MR images of Gd-DOTA-DEVD-Tfb with and without caspase-3 are shown in Figure 3. Caspase-3 activity induced a noticeable signal enhancement. This result is compatible with the one-dimensional ^{19}F NMR data shown in Figure 2b. We used a relatively high probe concentration for MRI because of the sensitivity limitation due to our current instrument setup. However, the intrinsically high sensitivity for the ^{19}F signal of the probe is demonstrated by the NMR spectra measured at 1−5 μM by a well-tuned spectrometer (Figure S5 in Supporting Information). This result indicates the possibility that a suitable instrument enables in vivo ^{19}F MR imaging in the future.

In conclusion, a novel design principle of ^{19}F MRI probes detecting protease activity was developed. This principle is based on MRI signal quenching from the intramolecular paramagnetic effect of Gd^{3+}. The intramolecular Gd^{3+} made the T_2 of the probe too short to be measured, with the paramagnetic effect which can be cancelled by the probe hydrolyzation by caspase-3. T_2 is a parameter that can be used to generate contrasts in MR images. Using this probe as a positive contrast agent, we demonstrated that the probe could detect caspase-3 activity spatially from the phantom image using ^{19}F MRI. This method could be applied to the sensing of not only other kinds of proteases but also other hydrolases such as nucleases and phosphodiesterases. It is expected that this sensing strategy might become the basis for the next stage of in vivo molecular imaging techniques.

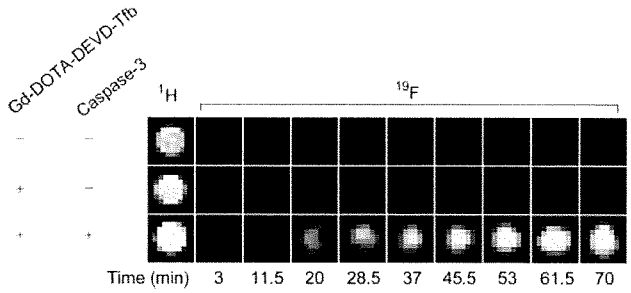

Figure 3. Time course of density-weighted ^{19}F MR images of Gd-DOTA-DEVD-Tfb (1 mM) with or without caspase-3 at 37 °C.

Acknowledgment. This work was supported by MEXT of Japan, by JST, by the Mitsubishi Foundation, by Kato Memorial Bioscience Foundation, by Astellas Foundation for Research on Metabolic Disorders, by the Uehara Memorial Foundation, by Terumo Life Science Foundation, by Nagase Science and Technology Foundation and by the Asahi Glass Foundation to K.K., by the Cosmetology Research Foundation to S.M., by CREST (JST) to M.S. We thank Dr. Tetsuro Kokubo at Yokohama City University for the use of MRI instrument.

Supporting Information Available: Detailed experimental procedures and supplementary results. This material is available free of charge via the Internet at http://pubs.acs.org.

References

(1) (a) Jasanoff, A. *Trends Neurosci.* **2005**, *28*, 120−126. (b) Sosnovik, D. E.; Weissleder, R. *Curr. Opin. Biotechnol.* **2007**, *18*, 4−10.
(2) (a) Zhang, S.; Kuangcong, W.; Sherry, A. D. *Angew. Chem., Int. Ed.* **1999**, *38*, 3192−3194. (b) Aime, S.; Barge, A.; Castelli, D. D.; Fedeli, F.; Mortillaro, A.; Nielsen, F. U.; Terreno, E. *Magn. Reson. Med.* **2002**, *47*, 639−648.
(3) (a) Li, W.; Fraser, S. E.; Meade, T. J. *J. Am. Chem. Soc.* **1999**, *121*, 1413−1414. (b) Hanaoka, K.; Kikuchi, K.; Urano, Y.; Narazaki, M.; Yokawa, T.; Sakamoto, S.; Yamaguchi, K.; Nagano, T. *Chem. Biol.* **2002**, *9*, 1027−1032.
(4) (a) Louie, A. Y.; Hüber, M. M.; Ahrens, E. T.; Rothbächer, U.; Moats, R.; Jacobs, R. E.; Fraser, S. E.; Meade, T. J. *Nat. Biotechnol.* **2000**, *18*, 321−325. (b) Perez, J. M.; Josephson, L.; O'Loughlin, T.; Högemann: Weissleder, R. *Nat. Biotechnol.* **2002**, *20*, 816−820. (c) Yoo, B.; Pagel, M. D. *J. Am. Chem. Soc.* **2006**, *128*, 14032−14033. (d) Chen, J. W.; Sans, M. Q.; Bogdanov, A.; Weissleder, R. *Radiology* **2006**, *240*, 473−481.
(5) Yu, J.; Kodibagkar, V. D.; Cui, W.; Mason, R. P. *Curr. Med. Chem.* **2005**, *12*, 819−848.
(6) Code, R. F.; Harrison, J. E.; McNeill, K. G.; Szyjkowski, M. *Magn. Reson. Med.* **1990**, *13*, 358−369.
(7) Higuchi, M.; Iwata, N.; Matsuba, Y.; Sato, K.; Sasamoto, K.; Saido, T. C. *Nat. Neurosci.* **2005**, *8*, 527−533.
(8) (a) Cui, W.; Otten, P.; Li, Y.; Koeneman, K. S.; Yu, J.; Mason, R. P. *Magn. Reson. Med.* **2004**, *51*, 616−620. (b) Yu, J.; Liu, L.; Kodibagkar, V. D.; Cui, W.; Mason, R. P. *Bioorg. Med. Chem.* **2006**, *14*, 326−333.
(9) Helm, L. *Prog. Nucl. Magn. Reson. Spectrosc.* **2006**, *49*, 45−64.
(10) Thornberry, N. A.; Rano, T. A.; Peterson, E. P.; Rasper, D. M.; Timkey, T.; Garcia-Calvo, M.; Houtzager, V. M.; Nordstrom, P. A.; Roy, S.; Vaillancourt, J. P.; Chapman, K. T.; Nicholson, D. W. *J. Biol. Chem.* **1997**, *272*, 17907−17911.

JA077058Z

DOI: 10.1002/chem.200700785

A Gd^{3+}-Based Magnetic Resonance Imaging Contrast Agent Sensitive to β-Galactosidase Activity Utilizing a Receptor-Induced Magnetization Enhancement (RIME) Phenomenon

Kenjiro Hanaoka,[a] Kazuya Kikuchi,[b] Takuya Terai,[a] Toru Komatsu,[a] and Tetsuo Nagano*[a]

Abstract: Magnetic resonance imaging (MRI) permits noninvasive three-dimensional imaging of opaque organisms. Gadolinium (Gd^{3+}) complexes have become important imaging tools as MRI contrast agents for MRI studies, though most of them are nonspecific and report solely on anatomy. Recently, MRI contrast agents have been reported whose ability to relax water protons is triggered or greatly enhanced by recognition of a particular biomolecule. This new class of MRI contrast agents could open up the possibility of reporting on the physiological state or metabolic activity deep within living specimens. One possible strategy for this purpose is to utilize the increase in the longitudinal water proton r_1 relaxivity that occurs upon slowing the molecular rotation of a small paramagnetic complex, a phenomenon which is known as receptor-induced magnetization enhancement (RIME), by either binding to a macromolecule or polymerization of the agent itself. Here we describe the design and synthesis of a novel β-galactosidase-activated MRI contrast agent, the Gd^{3+} complex **[Gd-5]**, by using the RIME approach. β-Galactosidase is commonly used as a marker gene to monitor gene expression. This newly synthesized compound exhibited a 57% increase in the r_1 relaxivity in phosphate-buffered saline (PBS) with 4.5% w/v human serum albumin (HSA) in the presence of β-galactosidase. Detailed investigations revealed that RIME is the dominant factor in this increase of the observed r_1 relaxivity, based on analysis of Gd^{3+} complexes **[Gd-5]** and **[Gd-8]**, which is generated from **[Gd-5]** by the activity of β-galactosidase, and spectroscopic analysis of their corresponding Tb^{3+} complexes, **[Tb-5]** and **[Tb-8]**.

Keywords: biosensors · gadolinium complexes · lanthanides · luminescence · magnetic resonance imaging

Introduction

Magnetic resonance imaging (MRI) is a noninvasive imaging technique that can provide images of intact, opaque organisms in three dimensions, even deep within a specimen, without photobleaching or light scattering which are often observed in light-based microscopy imaging experiments.[1] Therefore, MRI is useful not only in clinical medicine, but also in experimental research.[1,2] Nowadays, there is a considerable interest in MRI contrast agents, which can improve the resolution of MR images.[1,2] The MR images are based upon the NMR signal from water protons, and the signal intensity depends upon the water concentration and relaxation time (T_1 and T_2).[2] Paramagnetic ions like the gadolinium ion (Gd^{3+}), primarily shorten the T_1 (spin–lattice) relaxation time with high efficacy by rapid exchange of inner-sphere water molecules with bulk solvent.[3] Thus, Gd^{3+}-based MRI contrast agents increase tissue contrast by increasing water proton relaxation, and are widely used in clinical diagnostics.[4] In Gd^{3+}-based MRI contrast agents, chelation of Gd^{3+} is required for safety reasons: Dissociation of Gd^{3+} from a MRI contrast agent is undesirable, as both the free metal and unchelated ligands are generally more toxic than the complex itself.[2,4] Commonly used MRI

[a] Dr. K. Hanaoka, T. Terai, T. Komatsu, Prof. Dr. T. Nagano
Graduate School of Pharmaceutical Sciences
The University of Tokyo
7-3-1, Hongo, Bunkyo-ku, Tokyo 113-0033 (Japan)
Fax: (+81) 3-5841-4855
E-mail: tlong@mol.f.u-tokyo.ac.jp

[b] Prof. Dr. K. Kikuchi
Department of Materials and Life Sciences
Graduate School of Engineering, Osaka University
2-1 Yamada-oka, Suita City, Osaka 565-0871 (Japan)

Supporting information for this article is available on the WWW under http://www.chemeurj.org/ or from the author.

contrast agents are mainly extracellular agents with nonspecific biodistribution.[4,5] In contrast, it is also possible to develop Gd^{3+} complexes with various chemical properties by means of appropriate ligand design for Gd^{3+},[6] and, indeed, some bioactivated MRI contrast agents have been reported for monitoring enzyme activity, Ca^{2+}, pH, $p(O_2)$, Zn^{2+}, and so on.[7] These MRI contrast agents show a change in the water proton relaxation time (T_1 or T_2) in response to the presence of specific biomolecules. Recently, attempts have been made to utilize MR imaging techniques to detect gene expression, and the development of these methods would allow MR imaging of the expression of specific genes.[8] For example, β-galactosidase is a commonly used gene expression marker, that is, gene expression is monitored by introducing a marker gene, lacZ, to follow the regulation of a gene of interest because it can easily be assayed and is not normally expressed in most mammalian tissues or cells.[9] Meade and co-workers developed the bioactivated MRI contrast agent, EgadMe, which reports on β-galactosidase activity to image the expression of a transgene.[10] The mechanism of the T_1 relaxation time change between two distinct relaxation states, long and short, is as follows. The enzyme substrate, galactopyranose, which is linked to the ligand, blocks the one remaining open coordination site of the chelated Gd^{3+}, inhibiting access of water to the chelated Gd^{3+} ion. The contrast agent is switched on when β-galactosidase cleaves the galactopyranose from the Gd^{3+} complex and the chelated Gd^{3+} ion becomes accessible to water. This agent has been successfully used in vivo to monitor gene expression in *Xenopus laevis*.[10a] Thus, this MRI contrast agent showed a change in the longitudinal relaxation time (T_1) in the presence of β-galactosidase by modulating the access of water molecules to the chelated Gd^{3+} ion. In addition to above results, β-galactosidase-activated MRI contrast agents with a range of chemical properties are also needed for further biological studies, so the development of novel β-galactosidase-activated MRI contrast agents with a different design approach would be helpful for studies of biological phenomena by monitoring gene expression. One possible approach for the development of biomolecule-activated MRI contrast agents is the RIME (receptor-induced magnetization enhancement) approach.[11] The binding of a MRI contrast agent to a macromolecule substantially slows molecular rotation of the Gd^{3+} complex, resulting in an additional increase in the r_1 relaxivity through the rotational correlation time τ_R.[2] When the Gd^{3+} complex binds to a macromolecule, the τ_R increases from that of a small molecule to that of the protein, and the r_1 relaxivity increases. The slower the Gd^{3+} complex tumbles, the longer the τ_R, leading to faster relaxation rates and, hence, higher r_1 relaxivity. The τ_R for small Gd^{3+} complexes is usually in the picosecond range (typically 50–200 ps), whereas the τ_R for a macromolecule such as albumin is in the nanosecond range (about 50 ns).[6a] This phenomenon is known as RIME. RIME agents have been reported for alkaline phosphatase and for carboxypeptidase B (part of the thrombin-activatable fibrinolysis inhibitor family), which regulate noncovalent binding of the agents to human serum albumin (HSA).[12,13] Another agent permitted the detection of yeast transcription repressor protein (Gal80) as MR images by utilizing a specific peptide-protein binding event,[14] and the enzyme carbonic anhydrase was selectively targeted with a sulfonamide substituent.[15] Moreover, oligonucleotide sequences have also been detected with iron oxide nanoparticles derivatized with oligonucleotide.[16] Hybridization with oligonucleotide-derived particles resulted in changes mainly in the spin–spin relaxation time (T_2) of adjacent water protons. Efficient polymerization of Gd^{3+} complexes can also be used to directly image the activity of enzymes such as myeloperoxidase (MPO) and matrix metalloproteinase 2 (MMP-2).[17,18]

Here, we report the design and synthesis of a novel β-galactosidase-activated MRI contrast agent based on the RIME approach (Figure 1). Reaction with β-galactosidase

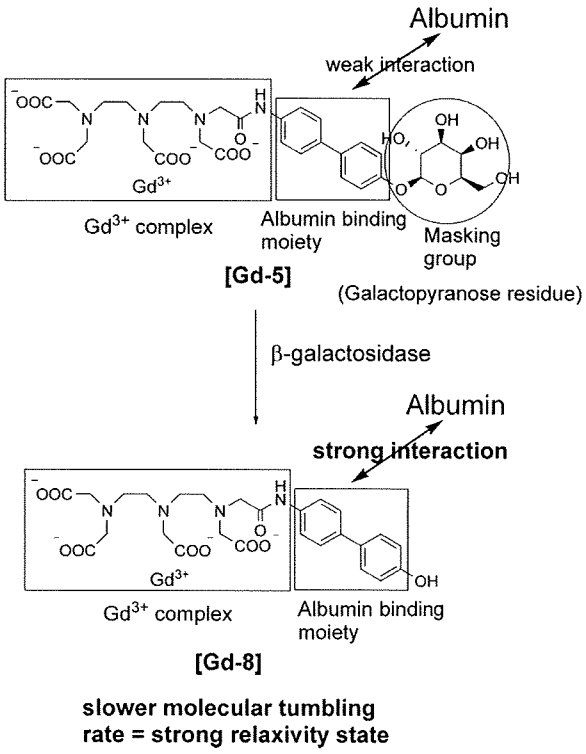

Figure 1. The RIME mechanism for the β-galactosidase-activated MRI contrast agent **[Gd-5]**. In **[Gd-5]**, a Gd^{3+} complex is coupled to an albumin binding moiety that is masked by the galactopyranose residue. The galactopyranose residue of **[Gd-5]** is designed to be cleaved by β-galactosidase, transforming **[Gd-5]** to **[Gd-8]**, and this cleavage promotes albumin binding of the Gd^{3+} complex.

yielded a 57% increase in the r_1 relaxivity in phosphate-buffered saline (PBS) with 4.5% w/v HSA. Cleavage of the galactopyranose moiety from the aryl group of the Gd^{3+} complex increases the hydrophobicity of the aryl group, thereby increasing the HSA binding affinity. The greater binding of the Gd^{3+} complex to the macromolecule, HSA, increases

the r_1 relaxivity. We also confirmed the mechanism of this increase in the r_1 relaxivity.

Results and Discussion

Design and synthesis of [Gd-5] and [Gd-8]: The Gd^{3+} complex, **[Gd-5]**, was designed to detect β-galactosidase activity through conversion of the MRI-silent agent into an activated MRI agent, **[Gd-8]** (Figure 1). The **[Gd-5]** is composed of three moieties: 1) a masking group consisting of galactopyranose; 2) an albumin-binding moiety, the biphenyl group; 3) an MRI signal-generating moiety, which is a Gd^{3+} complex. This design relies upon enzymatic transformation of a Gd^{3+} complex with poor albumin affinity and concomitant low relaxivity into one with high albumin affinity and high relaxivity. The biphenyl group was selected as the albumin binding group, because the biphenyl residue is known to possess high albumin binding affinity.[4,13,19] A substrate for β-galactosidase, galactopyranose, was used as a masking group, affording extremely high hydrophilicity compared with the hydrophobicity of the biphenyl group. Hydrolysis of the galactopyranose moiety unblocks the hydrophobicity of the biphenyl group, thereby increasing the albumin binding affinity. Thus, in **[Gd-5]**, a masking group that inhibits albumin binding was expected to be removed by the enzymatic activity, to expose an albumin-binding group with high affinity. The strong interaction of the Gd^{3+} complex with a macromolecule such as albumin increases the r_1 relaxivity owing to the RIME phenomenon. The synthetic schemes for the lanthanide complexes, **[Gd-5]** and **[Gd-8]**, and details of the chemical characterization of compounds are provided in the Supporting Information.

Longitudinal relaxation time T_1 measurements of [Gd-5] with β-galactosidase: The longitudinal relaxation times T_1 of **[Gd-5]** were measured in the presence of β-galactosidase or heat-inactivated β-galactosidase with 4.5% w/v HSA in phosphate-buffered saline (PBS; pH 7.4), at 20 MHz (0.47 T), at 37 °C (Figure 2). The value of $1/T_1$ increased from 3.5 to 5.5 s^{-1} between 0 and 250 min in the presence of β-galactosidase (113 nM), whereas the value of $1/T_1$ changed only slightly from 3.8 to 4.0 s^{-1} between 0 and 250 min on exposure to heat-inactivated β-galactosidase (113 nM). We also assessed the ability of β-galactosidase to remove the galactopyranose masking group from **[Gd-5]** by high-pressure liquid chromatography (HPLC) analysis (Figure 3).

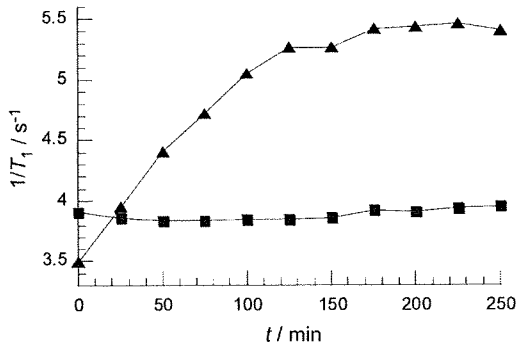

Figure 2. Time course of the β-galactosidase-induced (113 nM; ▲) and heat-inactivated β-galactosidase-induced (113 nM; ■) changes in the value of $1/T_1$ [s^{-1}], of 0.5 mM **[Gd-5]** solution at 20 MHz, 37 °C in phosphate-buffered saline (PBS; pH 7.4) with 4.5% w/v human serum albumin (HSA).

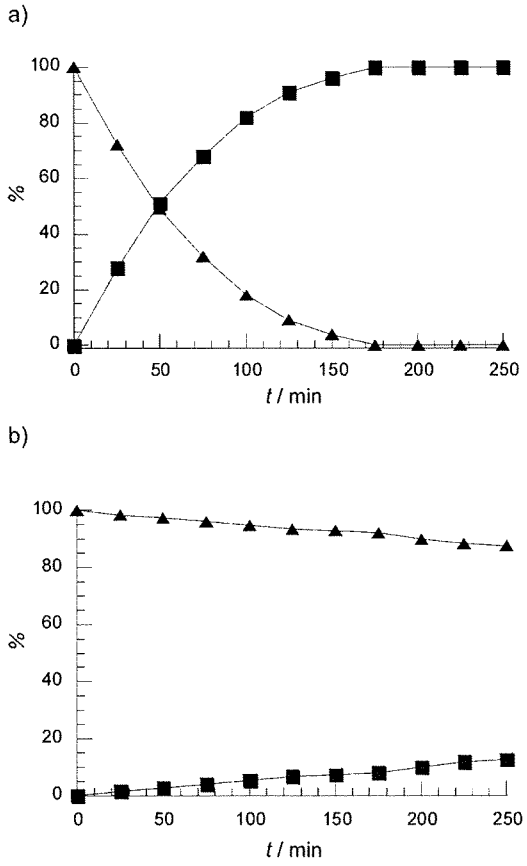

Figure 3. Time course of the conversion of **[Gd-5]** to **[Gd-8]**; the distribution of reaction species was quantified by HPLC analysis on the basis of the absorbance at 300 nm. The Gd^{3+} complex, **[Gd-5]** (0.5 mM) was incubated with: a) β-Galactosidase (113 nM) (**[Gd-5]**: ▲, **[Gd-8]**: ■) or; b) heat-inactivated β-galactosidase (113 nM) (**[Gd-5]**: ▲, **[Gd-8]**: ■) at pH 7.4, and 37 °C, in phosphate-buffered saline (PBS) in the presence of 4.5% w/v human serum albumin (HSA).

This HPLC analysis showed that the Gd^{3+} complexes, **[Gd-5]** and **[Gd-8]**, had distinct retention times, and **[Gd-5]** was converted into **[Gd-8]** in the presence of β-galactosidase (113 nM), whereas essentially no change was observed upon the addition of heat-inactivated β-galactosidase (113 nM). The HPLC experiments confirmed the enzymatic processing of **[Gd-5]** by the β-galactosidase. Thus, **[Gd-5]** exhibited a β-galactosidase-induced RIME effect, accompanying the removal of the galactopyranose residue of **[Gd-5]**.

The r_1 relaxivity of Gd^{3+} complexes, [Gd-5] and [Gd-8]: The paramagnetic species, Gd^{3+}, acts as a catalyst to relax bulk water protons by fast exchange of the coordinated

